Signatures of superconducting Higgs mode in irradiated Josephson junctions

Aritra Lahiri [1,*] Juan Carlos Cuevas [2,3,†] and Björn Trauzettel [1,4]

[1] *Institute for Theoretical Physics and Astrophysics, University of Würzburg, D-97074 Würzburg, Germany*

[2] *Departamento de Física Teórica de la Materia Condensada, Universidad Autónoma de Madrid, E-28049 Madrid, Spain*

[3] *Condensed Matter Physics Center (IFIMAC), Universidad Autónoma de Madrid, E-28049 Madrid, Spain*

[4] *Würzburg-Dresden Cluster of Excellence ct.qmat, Germany*

(Received 7 October 2025; revised 24 November 2025; accepted 2 January 2026; published 22 January 2026)

The Higgs mode, originally proposed in the context of superconductivity, corresponds to oscillations of the amplitude of the superconducting order parameter. Recent terahertz-domain optical studies have found signatures consistent with the Higgs mode, but its unambiguous detection is still challenging. We predict that the existence of the Higgs mode can be unambiguously revealed by standard measurements of the transport characteristics in microwave-irradiated asymmetric and transparent Josephson junctions. One signature of the Higgs mode in a Josephson junction is the microwave-induced enhancement of the second harmonic of the equilibrium current-phase relation (at zero dc bias voltage), whose sign differs from its expected value in the absence of the Higgs mode. As the radiation frequency is varied, this enhancement exhibits resonant behavior when the microwave frequency is tuned across the Higgs mass. The second signature that we propose is the enhancement of the second harmonic of the ac Josephson current at finite dc voltage bias, which can be probed in a customary analysis of the Shapiro steps in a microwave-irradiated junction.

DOI: 10.1103/njvs-s1p5

I. INTRODUCTION

Superconductors (SCs) are characterized by the spontaneous breaking of global $U(1)$ symmetry, resulting in a complex order parameter (OP) $\Delta(t) = |\Delta(t)| \exp(i\vartheta(t))$. In equilibrium, the amplitude of the OP, $|\Delta(t)|$, is static and results in a spectroscopic gap. Nevertheless, in a nonequilibrium dynamical scenario, it embodies a collective mode, namely, the Higgs mode [1–11]. Unlike the Nambu-Goldstone mode associated with the phase $\phi(t)$, which gets screened by electromagnetic fields and acquires a mass on the order of the plasma frequency [12], the Higgs mode is electrically neutral, which makes its detection challenging. Only recently have nonlinear electromagnetic excitation with terahertz (THz) spectroscopy signatures consistent with the Higgs mode been observed [6–9,11,13–15].

Alternatively, there have been a few theoretical studies predicting signatures of the existence of the Higgs mode in transport measurements [16–22], with some of them exploring a Josephson setup [21,23,24]. The Josephson effect [25], characterized by the coherent tunneling of Cooper pairs across a Josephson junction (JJ) of two superconducting leads, is a hallmark of phase coherence of the SCs. As such, the Josephson current serves as a proxy for the SC OP, and it may be expected to bear an imprint of the SC collective modes [4,23]. In particular, Refs. [4,26] have argued that the Josephson coupling between two SCs in a voltage (V)-biased JJ, which bears the form $\sim\Delta_{0,L}\Delta_{0,R}\cos(\phi)$, with $\Delta_{0,L/R}$ being the equilibrium gaps of the left(L)/right(R) leads and $d\phi/dt = d/dt(\vartheta_L - \vartheta_R) = 2$ eV the Josephson phase (we use $\hbar = 1$), provides a way to excite the Higgs mode at frequency equaling 2 eV. Subsequently, Ref. [24] proposed that the resulting signatures of the Higgs mode may be found in the ac Josephson current in voltage-biased JJs with high transparency even in the absence of external irradiation. Unlike the usual Josephson current, which oscillates at the Josephson frequency $\omega_J = 2$ eV for a constant dc voltage bias V, the Higgs mode manifests as a time-dependent component in the OP, which enhances the second-harmonic Josephson current at frequency $2\omega_J$. In junctions with highly asymmetric/unequal SC gaps on the two leads, along with high transparency, this Higgs-enhanced $2\omega_J$ current may even dominate the ω_J current, which constitutes a clear indication of the Higgs mode in conventional JJs with s-wave SCs, in the absence of time-reversal symmetry breaking [27–40].

The problem with these proposals is that a direct detection of such a Higgs-enhanced Josephson current is virtually impossible due to the very high required frequency [the Higgs frequency is set by the superconducting gap, which for Al SCs as an example would be on the order of 45 GHz]. To circumvent this problem we propose to follow the conventional way in which the ac Josephson effect is revealed, namely, via the measurement of the transport characteristics under microwave irradiation [41–46]. To be precise, we propose to investigate highly asymmetric and fairly transparent Josephson junctions irradiated by microwaves at frequency ω_r. We predict the following two unambiguous signatures of the existence of the Higgs mode in a JJ: First, in the absence of a dc voltage bias and for intermediate transparencies, the Higgs mode induces a significant enhancement of the second harmonic of

*Contact author: aritra.lahiri@uni-wuerzburg.de

†Contact author: juancarlos.cuevas@uam.es

 ©2026 American Physical Society

the microwave-assisted current-phase relation (CPR), which is otherwise typically dominated by the term $\sim\sin(\phi)$. On tuning ω_r across ω_H, this Higgs-induced second-harmonic component displays a resonant behavior, reflecting the underlying Higgs physics. Notably, the Higgs mode induces a sign change in the second harmonic of the CPR, which manifests in the full CPR as well. Second, when such asymmetric and transparent irradiated JJs are subjected to a dc voltage bias as well, besides the usual ac Josephson effect where the current develops harmonics of the Josephson frequency ω_J associated with the dc component of the voltage, it also develops harmonics of the radiation frequency. For voltages equaling rational multiples of the radiation frequency, $\omega_J = (n/m)\omega_r$ where n, m are integers, these components synchronize and constructively add to yield a dc current [41–43], appearing as Shapiro spikes/steps (SS) in the dc current-voltage characteristics (IVC). Crucially, the amplitudes of the SSs carry an imprint of the ac components of the Josephson current in the *absence* of the radiation. In this work, we extensively discuss these two signatures with the help of a microscopic theory that accounts for the self-consistent dynamics of the order parameter in microwave-irradiated junctions. With this theory, we demonstrate that microwave-assisted CPR, as well as Shapiro steps in a DC IVC measurement, both provide viable ways to detect the Higgs renormalized $2\omega_J$ Josephson current. Last, we remark that while Ref. [21] had considered a seemingly similar setup, it had some key differences. In Ref. [21], the bulk of the superconducting leads constituting the JJ are subjected to a uniform oscillating vector potential to induce the Higgs oscillations, which show up in the Josephson current. However, in typical junctions, the microwave radiation manifests as an oscillating voltage across the barrier, which is not equivalent to an oscillating vector potential permeating the leads. As we demonstrate below, this difference gives rise to qualitatively distinct OP dynamics, and hence, different CPR and SSs.

The rest of this paper is organized as follows: In Sec. II, we start with a phenomenological model to exlain the origin of the Higgs oscillations in microwave-irradiated JJs. We specialize to the case of microwave-assisted CPR in Sec. II A, followed by an exposition of SSs in Sec. II B, demonstrating in both cases how the Higgs mode manifests in the current. After a description of our microscopic Floquet-Keldysh formalism in Sec. III employed to rigorously analyze the Higgs signatures, we present the numerical results in Secs. IV A and IV B, exploring in detail the microwave-assisted CPR and SSs, respectively. Finally, we summarize our conclusions, and discuss some practical considerations, in Sec. V.

II. PHENOMENOLOGY

Before discussing the microscopic theory that allows us to quantitatively predict how the Higgs mode shows up in the transport characteristics of irradiated JJs, we illustrate in this section the underlying principles with a phenomenological model. For this purpose, we first recapitulate the key results of Ref. [24]. Conventional treatments of JJs employ BCS mean-field SC Hamiltonians with static/time-independent gap amplitudes. In contrast, on relaxing this constraint, we find that under suitable conditions, a self-consistent solution for the OP in JJs driven by microwave radiation and/or dc voltage bias acquires a time-dependent *amplitude* governed by the Higgs mode. Crucially, this should be distinguished from the more familiar case where the time dependence of the OP arises from a time-dependent *phase* but a static amplitude. Similar to the usual equilibrium/static proximity effect, wherein the gaps of two SCs in contact with each other are modified in the vicinity of the junction, these Higgs oscillations may be understood as a dynamical proximity effect between the two voltage-biased SCs. We demonstrate this with a phenomenological model of the two OPs coupled at the junction. We relegate the details to Appendix A, and summarize the key results here. Assuming without loss of generality that the left SC is at a potential $V(t)$ relative to the right SC, on decoupling the two SCs constituting the JJ, the OPs have the form $\Delta_{0,L/R}e^{-i\vartheta_{L/R}(t)}$, where $\vartheta_L(t) = \vartheta_{0,L} + \int_{-\infty}^{t} 2\,\mathrm{eV}(t')dt'$ and $\vartheta_R(t) = \vartheta_{0,R}$ [48,49]. This relative time dependence imprints upon the leading-order coupling between the OPs of the two SCs $\sim J\Re(\Delta_L(t)^*\Delta_R(t))$, where $J \sim \mathcal{T}^2$ with $\mathcal{T}$ being the tunnel coupling. For a dc voltage bias, this provides a stimulus at frequency 2 eV [26], which leads to the usual ac Josephson effect [25]. Additionally, the same time dependence enhances the usual proximity effect by eliciting a dynamical response; along with a change in the static gap amplitude, the OP also acquires a time-dependent part whose spectrum derives from the time dependence of the coupling. Throughout this work, we consider highly asymmetric JJs with $\Delta_{0,L} < \Delta_{0,R}$ without loss of generality, where the external drive excites the Higgs mode only in the left SC. Expanding the OP amplitude in the left SC as $\Delta_L(t,x) = \Delta_{0,L}(x) + \delta\Delta_L(t,x)$, with $\delta\Delta_L(t,x)$ capturing the time dependence, and the left lead occupying $x \leqslant 0$, we find that to the leading order in J [24]

$$\delta\Delta_L(\omega,q) = \chi_L(\omega,q)X_L(\omega), \tag{1a}$$

$$X_L(\omega) = \int \frac{dt}{2\pi} e^{i\omega t} 2J\Delta_{0,R}\cos\big(\phi(t)\big), \tag{1b}$$

$$\chi_L(\omega,q) = \frac{1}{-(\omega+i0)^2 + \omega_{H,L}(q)^2}. \tag{1c}$$

Here, $\phi(t) = \vartheta_L(t) - \vartheta_R(t)$ is the Josephson phase, $X_L(\omega)$ captures the dynamic excitation provided by the coupling between the two OPs, and $\chi_L(\omega,q)$ is the Higgs susceptibility of the left SC, which is peaked at the Higgs dispersion frequency $\omega = \omega_{H,L}(q) = 2\Delta_{0,L} + c^2q^2$, where q is the wave vector and c is the Higgs velocity. A detailed treatment of Higgs-mode damping lies beyond the scope of this phenomenological analysis. Consequently, the present results are not expected to remain valid when the drive frequency ω approaches or exceeds $\omega_{H,L}$. This limitation, however, does not apply to the microscopic numerical analysis which follows this section. Nevertheless, we find that certain key qualitative features are captured by our phenomenological analysis. As introduced earlier, we now propose two ways to excite the Higgs mode: (i) phase bias, and (ii) dc voltage bias, with both cases involving a microwave irradiation. These are described in the following subsections.

A. Phase bias: Current-phase relation

Let us first assume that the JJ is subjected to microwave radiation in the presence of a phase bias, but in the absence of a dc voltage bias. The radiation imposes an ac voltage $V_{\rm ac}\cos(\omega_r t)$ [41–46], which corresponds to the Josephson phase,

$$\phi(t) = \phi_0 + \underbrace{(2eV_{AC}/\omega_r)}_{:=\alpha}\sin(\omega_r t), \tag{2}$$

where ϕ_0 denotes the phase bias. Henceforth, we use $\alpha = 2\ eV_{\rm ac}/\omega_{\rm r}$ to parametrize the strength of the radiation. Before turning to the Higgs response, we first examine the trivial case where it is absent. We start with the "adiabatic" approximation (AA) [42,51]. The starting point in this approximation is the expression for the equilibrium Josephson current in the absence of microwaves, which is given by $I = \sum_n I^{(n)}\sin(n\phi_0)$. A microscopic analysis shows that the harmonics $I^{(n)}$ progressively decrease with increasing n, $|I^{(n)}| > |I^{(n+1)}|$, and contribute noticeably only at high transparencies. Additionally, their signs alternate, $\mathrm{sgn}(I^{(n)}) = -\mathrm{sgn}(I^{(n-1)})$, with $I^{(1)} > 0$, $I^{(2)} < 0$, and so on. The leading term, $I^{(1)} \sim J\Delta_{0,L}\Delta_{0,R}$, determines the critical current in the tunnel limit. The AA that describes the supercurrent in the presence of microwaves simply consists of substituting the time-dependent phase of Eq. (2) in the equilibrium CPR. This leads to the generalized result: $I = \sum_n \bar{I}^{(n)}\sin(n\phi_0)$, where the amplitudes $\bar{I}^{(n)}$ incorporate the effect of the microwaves and are related to the equilibrium amplitudes $I^{(n)}$ as we specify below. This type of approximation only works for slowly varying $\phi(t)$, which permits us to neglect the frequency dependence of $\bar{I}^{(n)}$ and replace them with their zero-frequency values [42,51]. In the presence of microwave radiation, we obtain on using Eq. (2) that

$$I = \sum_n \sum_a I^{(n)} J_a(n\alpha)\sin(n\phi_0 + a\omega_r t). \tag{3}$$

The dc supercurrent follows as

$$I = \sum_n \underbrace{I^{(n)}J_0(n\alpha)}_{\bar{I}^{(n)}}\sin(n\phi_0), \tag{4}$$

defining $\bar{I}^{(n)} = I^{(n)}J_0(n\alpha)$. Specifically, we note that the second-harmonic component, $\bar{I}^{(2)}$, depends on α as $J_0(2\alpha)$, and $\bar{I}^{(2)}(\alpha = 0) < 0$.

Returning to the case with Higgs renormalization, we shall now see that the $J_0(2\alpha)$ profile, as well as the sign of $\bar{I}^{(2)}(\alpha = 0)$ obtained above for the second-harmonic current, is altered significantly. Plugging Eq. (2) in Eqs. (1a)–1(c), we obtain the change in the OP as

$$\delta\Delta_L(t,x) = \sum_m \delta\Delta_{L,m}(x)e^{-im\omega_r t}, \tag{5a}$$

$$\delta\Delta_{L,m}(q) = \begin{cases}\cos(\phi_0)J_m(\alpha)\chi_L(m\omega_r,x) & m:\text{even}\\ -i\sin(\phi_0)J_m(\alpha)\chi_L(m\omega_r,x) & m:\text{odd}\end{cases}, \tag{5b}$$

$$\chi_L(\omega,x) = \sum_q \chi_L(\omega,q)e^{iqx} = \frac{e^{-\frac{|x|\sqrt{\omega_{H,L}^2-\omega^2}}{c}}}{2c\sqrt{\omega_{H,L}^2-(m\omega_r)^2}}. \tag{5c}$$

This shows that the OP contains harmonics of ω_r, which are resonantly excited when the harmonic frequency $m\omega_r$ matches the Higgs frequency ω_H. The higher harmonics decay parametrically due to the factor $J_m(\alpha)$. We reiterate that this analysis is only valid for small $\omega_r \ll \omega_{H,L}$, along with $\alpha < 1$, due to the limitations of the AA and the phenomenological field theory for the coupled OPs. Within the AA, promoting the equilibrium supercurrent to $I \sim J\Delta_L(t)\Delta_{0,R}\sin(\phi(t))$ and using Eq. (5), the dc supercurrent once again bears the form given by Eq. (4), albeit with the Higgs-renormalized amplitudes $\bar{I}^{(n),\rm Higgs}$. In particular, while the first harmonic remains unchanged, the amplitude of the second harmonic, which encodes the Higgs renormalization, becomes

$$\bar{I}^{(2),\rm Higgs} \sim J\sum_m (-1)^m \frac{[J_m(\alpha)]^2}{\sqrt{\omega_{H,L}^2-(m\omega_r)^2}}. \tag{6}$$

From this, we can distinguish the Higgs resonance when harmonics of ω_r equal $\omega_{H,L}$, and the dependence on α. We find that the latter is equally helpful in indicating the underlying Higgs renormalization. Importantly, along with the difference in the α dependence with [Eq. (6)] and without [Eq. (4)] the Higgs renormalization, we note that $\bar{I}^{(2),\rm Higgs}(\alpha = 0) > 0$, in contrast to the Higgs-free case where $\bar{I}^{(2)}(\alpha = 0) < 0$, as mentioned earlier. This difference in the sign of the second-harmonic component plays a significant role in qualitatively altering the CPR, skewing the peak current. This is easy to see on retaining only the first two harmonics, yielding the current $I(\gamma,\phi_0) = \bar{I}^{(1)}\sin(\phi_0) + \gamma\sin(2\phi_0)$ (where γ is a weighting factor), which satisfies $I(\gamma,\phi_0) = I(-\gamma,\pi - \phi_0)$. Irrespective of the magnitude of the Higgs-renormalized second-harmonic component, the qualitative differences in the CPR, arising from the opposite sign of the second harmonic and its distinct αdependence, serve as a clear fingerprint of Higgs renormalization.

We emphasize that a reliable estimate of the second-harmonic amplitude requires a microscopic analysis, since for any finite α multiple harmonics of ω_r contribute, with the higher ones extending beyond $\omega_{H,L}$ where Higgs-mode damping becomes relevant. Nonetheless, as shown below, the α dependence predicted here agrees with our microscopic numerical results.

B. Voltage bias: Shapiro steps

Next, we consider the case of a microwave-irradiated JJ when a finite dc voltage biased is applied as well. For the discussion of this problem, it is convenient to first analyze the behavior of the OP and the Josephson current without microwave radiation, and then incorporate the effects of the radiation afterward. For a pure dc voltage bias corresponding to $\phi(t) = \phi_0 + 2\ eV\ t$, from a similar analysis as above [24], we find that as the voltage increases and $\omega_J \to \omega_{H,L}$, the left OP modulation is amplified by the Higgs resonance,

$$\delta\Delta_L(t,x) = J\chi_L(\omega,x)\cos(\omega_J t + \phi_0), \tag{7}$$

where $\chi_L(\omega,x)$ is shown in Eq. (5) above, while the off-resonant $\delta\Delta_R$ remains negligible. In this case, using the AA for the current as before, we see that it acquires a component oscillating at frequency $2\omega_J$, $I_{2\omega_J} = I_{\omega_J}f_H$, where

$I_{\omega_J} = J\Delta_{0,L}\Delta_{0,R}$ is the amplitude of the usual ω_J component obtained from the Ambegaokar-Baratoff relation [52], and $f_H \sim 1/\sqrt{\omega_{H,L}^2 - \omega_J^2}$ shows a resonant behavior as ω_J approaches the Higgs frequency. As we show below, this Higgs renormalized $I_{2\omega_J}$ may be inferred from Shapiro steps in irradiated JJs.

In the presence of both dc voltage bias and microwave radiation, the net voltage across the junction is given by $V + V_{\rm ac}\cos(\omega_r t)$. The corresponding Josephson phase becomes

$$\phi(t) = \phi_0 + \omega_J t + \alpha\sin(\omega_r t). \tag{8}$$

First we consider the case without any Higgs renormalization. Using the AA described above, the current reads

$$\begin{aligned} I(t) &= J\Delta_{0,L}\Delta_{0,R}\sin(\phi(t)) \\ &= \sum_n \underbrace{J\Delta_{0,L}\Delta_{0,R}}_{I_{\omega_J}} J_b(\alpha)\sin(\phi_0 + \omega_J t + b\omega_r t). \end{aligned} \tag{9}$$

From this current, we obtain the bth SS when $\omega_J = |b|\omega_r$, with maximum height $SS_b^1 = I_{\omega_J}J_{-|b|}(\alpha)$. For convenience, we have defined SS_b^a to refer to the SS at $a\omega_J = b\omega_r$. Specifically,

$$SS_1^1 = 2\max_{\phi_0}[I_{\omega_J}J_{-1}(\alpha)\sin(\phi_0)] = 2I_{\omega_J}J_{-1}(\alpha), \tag{10}$$

which has a characteristic $J_{-1}(\alpha)$ profile as a function of α. Note that this reveals the amplitude of the ac Josephson current at *zero* ac voltage, I_{ω_J}. For high transparencies, equivalently large J, the higher harmonics $I_{a\omega_J}$ oscillating at frequency $a\omega_J$ may also be significant. Specifically, on including the $2\omega_J$ current,

$$\begin{aligned} I(t) = &\sum_n I_{\omega_J}J_b(\alpha)\sin(\phi_0 + \omega_J t + b\omega_r t) \\ &+ \sum_{b'} I_{2\omega_J}J_{b'}(2\alpha)\sin(2\phi_0 + 2\omega_J t + b'\omega_r t), \end{aligned} \tag{11}$$

two changes occur: (i) The previously obtained SS_b^1 are modified as the second line in Eq. (11) contributes to SS_b^1 when $2\omega_J = (b' = 2b)\omega_r$. This yields

$$SS_1^1 = 2\max_{\phi_0}[I_{\omega_J}J_{-1}(\alpha)\sin(\phi_0) + I_{2\omega_J}J_{-2}(2\alpha)\sin(2\phi_0)]. \tag{12}$$

Notice that $I_{2\omega_J}$ introduces a $J_{-2}(2\alpha)$ dependence, deviating from the $J_{-1}(\alpha)$ obtained earlier in Eq. (10). This is noticeable as $J_{-2}(2\alpha)$ oscillates approximately twice as fast as $J_{-1}(\alpha)$. (ii) Another set of SSs, SS_b^2, is obtained when $2\omega_J = b\omega_r$ for odd b. Specifically, SS_1^2 has the height

$$SS_1^2 = 2\max_{\phi_0}[I_{2\omega_J}J_{-1}(2\alpha)\sin(2\phi_0)] = 2I_{2\omega_J}J_{-1}(2\alpha). \tag{13}$$

Typically, $I_{2\omega_J} \ll I_{\omega_J}$, particularly in highly asymmetric JJs as we shall see below, which results in $SS_1^2 \ll SS_1^1$ in the absence of Higgs renormalization.

Returning to the case with Higgs renormalization, the underlying Shapiro physics remains unaltered; what changes is the amplitude of $I_{2\omega_J}$. Within the simple AA, with $\Delta_{0,L} \ll \Delta_{0,R}$ and considering a dc voltage resonant with the Higgs mode of the left lead $\omega_J \approx 2\Delta_{0,L}$, we obtain $\delta\Delta_L(t) = \delta\Delta_L\cos(\phi(t))$ and $\delta\Delta_R \approx 0$. The resulting current is given by $I \sim J\Delta_L(t)\Delta_{0,R}\sin(\phi(t))$ [24]. Since by arguments of gauge invariance, the left OP responds as $\delta\Delta_L(t) = \delta\Delta_L\cos(\phi(t))$, the Higgs-renormalized current becomes

$$\begin{aligned} I(t) &= J[\Delta_{0,L} + \delta\Delta_L\cos(\phi(t))]\Delta_{0,R}\sin(\phi(t)) \\ &= \sum_b I_{\omega_J}J_b(\alpha)\sin(\phi_0 + \omega_J t + b\omega_r t) \\ &\quad + \sum_{b'} \underbrace{J\delta\Delta_L\Delta_{0,R}}_{I_{2\omega_J}^{\rm Higgs}} J_{b'}(2\alpha)\sin(2\phi_0 + 2\omega_J t + b'\omega_r t). \end{aligned} \tag{14}$$

Consequently, on enforcing the condition for SS_1^1 along with that of the Higgs resonance, i.e., $\omega_r = \omega_J = 2\Delta_{0,L}$, we obtain the same expression as Eq. (12), albeit with a much stronger Higgs enhancement $I_{2\omega_J}^{\rm Higgs} \gg I_{2\omega_J}$,

$$SS_1^1 = 2\max_{\phi_0}\left[I_{\omega_J}J_{-1}(\alpha)\sin(\phi_0) + I_{2\omega_J}^{\rm Higgs}J_{-2}(2\alpha)\sin(2\phi_0)\right]. \tag{15}$$

Similarly,

$$SS_1^2 = 2\max_{\phi_0}\left[I_{2\omega_J}^{\rm Higgs}J_{-1}(2\alpha)\sin(2\phi_0)\right]. \tag{16}$$

Note that $I_{2\omega_J}^{\rm Higgs}$ depends on the dc voltage. It is peaked at the Higgs resonance $\omega_J \approx \omega_{H,L}$. With an experiment probing the SS heights over a range of $V_{\rm ac}$, there are two distinct markers indicative of a Higgs-enhanced $2\omega_J$ current: (i) The relative magnitudes of SS_1^2 and SS_1^1 provide an estimate of the strength of the Higgs-renormalized $I_{2\omega_J}$, which is expected to enhance SS_1^2. In conventional JJs without any Higgs renormalization, the only other source of SS_1^2 is the higher-order Josephson effect arising from a large transparency. In this work, even though we consider transparencies up to $\approx$0.48, we find that the higher-order Josephson effect is much weaker than the corresponding Higgs-induced result, particularly in case of highly asymmetric JJs which, as we show below, suppress $I_{2\omega_J}$. (ii) A resonantly peaking behavior of SS_1^2 on sweeping ω_J across $\omega_{H,L}$ provides an unambiguous signature of the resonant Higgs renormalization of $I_{2\omega_J}$. Equivalently, the deviation of SS_1^1 from the $J_{-1}(\alpha)$ profile due to the contribution of $I_{2\omega_J}$, which introduces a $J_{-2}(2\alpha)$ component, is also expected to show a resonant enhancement across the Higgs resonance.

Let us emphasize that although this simplified analysis captures the essential physics, its validity is restricted to tunnel JJs subjected to radiation of sufficiently low frequency and intensity. Noting that the OP varies at the same timescale as ϕ, along with the fact that we consider high transparencies and radiation strength $V_{\rm ac}$, it is imperative to account for the proper retarded dynamics when obtaining the microscopic current [43,51,53–56]. We pursue a microscopic Keldysh formulation in the rest of our work, following Refs. [24,43]. Nevertheless, as we show later, the AA introduced above captures the salient features concerning the dependence of the step heights on the radiation strength.

III. MICROSCOPIC MODEL

Our technical formulation follows from Refs. [24] and [43], based on a self-consistent Keldysh-Gorkov framework [22,57–62]. We, nevertheless, describe the crucial aspects to

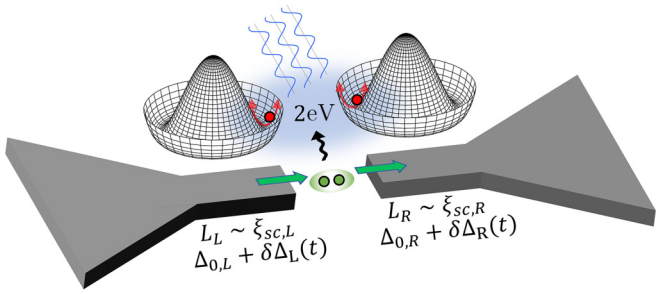

FIG. 1. Illustration of the JJ, with two leads of length $L_{L/R} \sim \xi_{SC,L/R}$ comparable to the superconducting coherence length (subscript L/R denotes left/right) forming a bridge. The outer ends of the leads are connected to macroscopic superconducting reservoirs (widening triangles). The JJ has high transparency, and it is highly asymmetric with unequal equilibrium gaps, $\Delta_{0,L} \ll \Delta_{0,R}$ without loss of generality. We find that the OP develops a time-dependent component, denoted $\delta\Delta_{L/R}(t)$, representing the Higgs mode. This Higgs mode, corresponding to radial oscillations of the OP (red balls) in the free-energy landscape of the OP (Mexican hat), is excited by radiating tunneling Cooper pairs. An external radiation (blue waves) may be used to alter the current-phase relation, or create Shapiro steps, which reveal the presence and the strength of the Higgs-induced Josephson current.

keep the discussion self-contained. We model our junctions with s-wave BCS SC Hamiltonians [24,53–56,63–66]. The device, as illustrated in Fig. 1, is a superconducting bridge comprising two SC leads of length L with $\lambda_F \ll L \sim \xi_{SC}$, where λ_F is the Fermi wavelength, and ξ_{SC} is the SC coherence length. This is because the Higgs oscillations take effect over a length scale $\sim\xi_{SC}$. The leads terminate in macroscopic SC reservoirs [67]. For numerical tractability, we consider a single-channel JJ. This is a valid assumption for specular tunneling across the interface, which establishes a homogeneous OP along the direction(s) transverse to current transport. This was already established in Ref. [24], albeit in the absence of external radiation. The *time-dependent* mean-field Hamiltonian, written in a local real-space basis, is given by $H = H_L + H_R + H_{\mathcal{T}}$, where

$$H_{L/R} = \sum_{j\in L/R,\sigma} (-\zeta c^\dagger_{j+1\sigma} c_{j\sigma} - \zeta c^\dagger_{j\sigma} c_{j+1\sigma}) + (\Delta_j(t) c^\dagger_{j\sigma} c^\dagger_{j\sigma'} + \Delta^*_j(t) c_{j\sigma'} c_{j\sigma}), \tag{17}$$

and

$$H_{\mathcal{T}} = \sum_\sigma (W(t) c^\dagger_{R1\sigma} c_{LN_L\sigma} + \text{H.c.}), \quad W(t) = -\mathcal{T} e^{i\frac{\phi(t)}{2}}. \tag{18}$$

Here, j labels sites belonging to the L(left) and R(right) leads, containing N_L and N_R sites, respectively. Furthermore, ζ denotes the hopping amplitude, with the bandwidth equaling 4ζ, $g > 0$ is the BCS attractive interaction, $\mathcal{T}$ denotes the junction tunnel coupling, and last $\phi(t)$ is given by either Eq. (2) or (8) depending on the biasing condition. We remark that by allowing the gaps $\Delta(t)$ to be time dependent, this formulation is able to capture the mean-field dynamics of the OP deriving from the Higgs mode. As described in Appendix A, following Refs. [4,24], the Josephson coupling stabilizes the Higgs fluctuations, shifting the OP's vacuum expectation value from the equilibrium static gap Δ_0 to a time-dependent one, $\Delta_0 + \delta\Delta(t)$. The latter is effectively captured by such a time-dependent mean-field formulation [22,60–62]. Additionally, in the Hamiltonian mentioned above, we have adopted a gauge in which the voltage is shifted from the chemical potentials, and it appears exclusively in the tunneling term [68]. There are two aspects to the validity of this procedure. First, even in equilibrium, a supercurrent flow establishes a phase gradient within the leads. In our setup, it can be shown that variation of the SC phase in the leads over a distance ξ_{SC} satisfies $\xi_{SC}\nabla\phi \sim \tau$, where τ is the normal-state transparency. Hence, for highly asymmetric junctions where the requirement of very high transparencies may be relaxed, it is justified to neglect the phase variations within the leads [24]. The macroscopic superconducting reservoirs, by virtue of the macroscopic number of transport channels, is immune to this issue. Second, beyond equilibrium, the presence of electric fields within the leads could lead to a time-varying phase. We consider type-I SCs with $\xi_{SC} \gg \Lambda$, where Λ is the penetration depth. Since the Higgs and transport physics occur over length scales $\sim\xi_{SC}$, it is safe to neglect the fields and the associated phase variations. Hence, we assume that the voltage drop is confined to the barrier.

For the dc voltage-biased and irradiated junction, the tunnel amplitude equals

$$W(t) = \sum_{m,n} \underbrace{-\mathcal{T} e^{-i\frac{\phi_0}{2}} \delta_{m,1} J_n\left(\frac{\alpha}{2}\right)}_{W_{mn}} e^{-im\frac{\omega_J}{2}t - in\omega_r t}, \tag{19}$$

revealing that energy is transferred in units of $\omega_J/2$ and ω_r. The tunneling self-energy is given by

$$\Sigma^{r/a}_{\mathcal{T},RL}(t) = \Sigma^{r/a}_{\mathcal{T},LR}{}^*(t) = W(t)\tau_+ - W^*(t)\tau_-, \tag{20a}$$

$$\Sigma^{r/a}_{\mathcal{T},RL;pq,mn} = W_{(p-m)(q-n)}\tau_+ - W^*_{(-(p-m))(-(q-n))}\tau_-, \tag{20b}$$

where τ denotes the Pauli matrices in Nambu space with $\tau_\pm = (\tau_0 \pm \tau_3)/2$. Since the OP responds to the energy supplied by the tunneling pairs, we have

$$\delta\Delta_j(t) = \sum_{m,n} \delta\Delta_{mn;j} e^{-im\frac{\omega_J}{2}t - in\omega_r t}, \tag{21}$$

with the corresponding self-energy being

$$\Sigma^{r/a}_{\delta\Delta,j}(t) = \delta\Delta_j(t)\tau_1, \tag{22a}$$

$$\Sigma^{r/a}_{\delta\Delta;pq,mn;j} = \delta\Delta_{(p-m)(q-n);j}\tau_1, \tag{22b}$$

where j denotes the spatial indices. Therefore, the two-time retarded and advanced Green functions may be written as (see Appendix B)

$$G^{r/a}(t,t') = \sum_{p,q} \int_{-\infty}^{\infty} \frac{d\omega}{2\pi} \overbrace{G^{r/a}\left(\omega + p\frac{\omega_J}{2} + q\omega_r, \omega\right)}^{G^{r/a}_{pq}(\omega)} \times e^{-i(\omega + p\frac{\omega_J}{2} + q\omega_r)t + i\omega t'}. \tag{23}$$

In this representation, the Dyson equations for the retarded and advanced components become

$$G^{r/a}_{pq}(\omega) = g^{r/a}_{00}(\omega)\delta_{p,0}\delta_{q,0} + \sum_{mn} g^{r/a}_{pq}(\omega)\Sigma^{r/a}_{pq,mn}G^{r/a}_{mn}(\omega), \tag{24}$$

where all quantities are matrices in Nambu space, and the bare Green function $g_{pq}(\omega) = g(\omega + p\omega_J/2 + q\omega_r)$ is defined in the absence of tunneling. The self-energy contains several contributions. Note that $\Sigma^{<}_{\mathcal{T}} = \Sigma^{<}_{\delta\Delta} = 0$ [68]. We also have the reservoir self-energy, $\Sigma^{r/a/<}_{\text{res.};pq,mn} = \zeta^2\tau_3 g_b^{r/a/<}\tau_3\delta_{p,m}\delta_{q,n}$, where g_b is the boundary Green function [67], acting only on the lead sites immediately neighboring the reservoir. Last, we include the broadening self-energy $\Sigma^{r/a}_{\Gamma;pq,mn} = \mp i(\Gamma/2)\delta_{p,m}\delta_{q,n}$ and $\Sigma^{<}_{\Gamma;pq,mn} = i\Gamma f(\omega)\delta_{p,m}\delta_{q,n}$, where $f(\omega)$ is the Fermi function. It aids numerical convergence, and accounts for the lifetime arising from, e.g., relaxation to the quasiparticle continuum, electron-phonon interaction, etc. [56]. Finally, the lesser Green function, which is central to our calculation, is obtained as [57,69–75]

$$G^{<}_{mn}(\omega) = \sum_{r,s} G^{r}_{(r+m)(q+n)}(\omega)\Sigma^{<}(\omega)G^{r\dagger}_{rs}(\omega), \tag{25}$$

where $G^{a}_{rs}(\omega) \equiv G^{a}(w, \omega + r\omega_J/2 + s\omega_r) = G^{r\dagger}(\omega + r\omega_J/2 + s\omega_r, w) \equiv G^{r\ \dagger}_{rs}$.

The nonequilibrium gap equation [22,24,57,59,61] becomes

$$\begin{aligned}\Delta_j(t) &= iu_{\text{BCS}}[G^{<}_{j,j}]_{1,2}(t,t)\\ \Rightarrow \Delta_{mn;j} &= iu_{\text{BCS}}\int_{-\infty}^{\infty}\frac{d\omega}{2\pi}[G^{<}_{mn,00;j,j}]_{1,2}(\omega),\end{aligned} \tag{26}$$

where u_{BCS} is the BCS interaction in the pairing channel, j denotes the spatial index, m and n denote the harmonics of $\omega_J/2$ and ω_r, respectively, and we consider the anomalous component of $G^{<}$, as evident from the subscript 1,2.

We self-consistently solve Eqs. (24)–(26) to obtain the OP. Finally, the current is obtained as [24,43]

$$I(t) = \sum_{mn} I_{mn}e^{-im\frac{\omega_J}{2}-in\omega_r t} \tag{27a}$$

$$\begin{aligned}I_{mn} = \sum_{p,q} e\int_{-\infty}^{\infty}\frac{d\omega}{2\pi}\mathbf{tr}[\tau_3\Sigma_{\mathcal{T},LR,(p+m),(q+n)}G^{<}_{R1LN_L,pq}(\omega)\\ -(L\leftrightarrow R)].\end{aligned} \tag{27b}$$

We note that the dc current is obtained as I_{00}, while the ac components oscillating at frequency ω_J and $2\omega_J$ are $I_{20} = I_{\omega_J}$ and $I_{40} = I_{2\omega_J}$, respectively. We use these notations interchangeably in this work.

As introduced above, we consider two observables, namely, the CPR and the SSs. The calculation of the SS amplitudes requires a full account of the Floquet indices corresponding to both dc and ac components of the voltage, exactly following the theory in this section. Recalling that SS^a_b is obtained when $a\omega_J = b\omega_r$, we obtain

$$\begin{aligned}SS^a_b = 2\max_{\phi_0}\Big[\sum_k \Im(I_{2ak,-bk} - I_{-2ak,bk})\sin(k\phi_0)\\ +\Re(I_{2ak,-bk} + I_{-2ak,bk})\cos(k\phi_0)\Big],\end{aligned} \tag{28}$$

where the first and the second lines correspond, respectively, to the sine and cosine Josephson currents [76].

The calculation of the CPR is simpler; while the procedure described above remains unchanged, the absence of the dc voltage bias ($\omega_J = 0$) lets us drop the corresponding Floquet indices altogether, with the time dependence of all quantities occuring only in harmonics of ω_r. For clarity, we summarize the details. The OP becomes

$$\delta\Delta_j(t) = \sum_n \delta\Delta_{n;j}e^{-in\omega_r t}. \tag{29}$$

With the self-energies now given by

$$\Sigma^{r/a}_{\mathcal{T},RL;q,n} = W_{(q-n)}\tau_+ - W^*_{-(q-n)}\tau_-, \tag{30a}$$

$$\Sigma^{r/a}_{\delta\Delta;q,n;j} = \delta\Delta_{(q-n);j}\tau_1, \tag{30b}$$

the Green functions admit the form

$$\begin{aligned}G^{r/a/<}(t,t') = \sum_q\int_{-\infty}^{\infty}\frac{d\omega}{2\pi}\overbrace{G^{r/a/<}(\omega+q\omega_r,\omega)}^{G^{r/a/<}_q(\omega)}\\ \times e^{-i(\omega+q\omega_r)t+i\omega t'}.\end{aligned} \tag{31}$$

Note that as shown in Appendix B, this is equivalent to the usual Floquet expansion. Consequently, the current is obtained as

$$I(t) = \sum_n I_n e^{-in\omega_r t}, \tag{32a}$$

$$\begin{aligned}I_n = \sum_q e\int_{-\infty}^{\infty}\frac{d\omega}{2\pi}\mathbf{tr}\big[\tau_3\Sigma_{\mathcal{T},LR,(q+n)}G^{<}_{R1LN_L,q}(\omega)\\ -(L\leftrightarrow R)\big].\end{aligned} \tag{32b}$$

The CPR is the dc component of the current, obtained from its zeroth Floquet component, I_0.

IV. RESULTS

In this section, we present our numerical results for the CPR, and the SSs, following the theory developed in the previous sections. We highlight the signatures of the Higgs mode in each case, contrasting with the corresponding results in the absence of the Higgs mode.

Throughout this work, we use a system of size $N_L = 18$, $N_R = 5$, $\mathcal{T}/\zeta = 0.4$ corresponding to the transparency ≈0.48 [43], $\Gamma/\Delta_{0,R} = 0.0125$, along with a BCS coupling constant, which leads to $\Delta_{0,R}/\zeta = 0.2$. The remaining parameters specific to each figure are specified in the corresponding captions. We discuss further practical considerations concerning the essential parameters below in Sec. V.

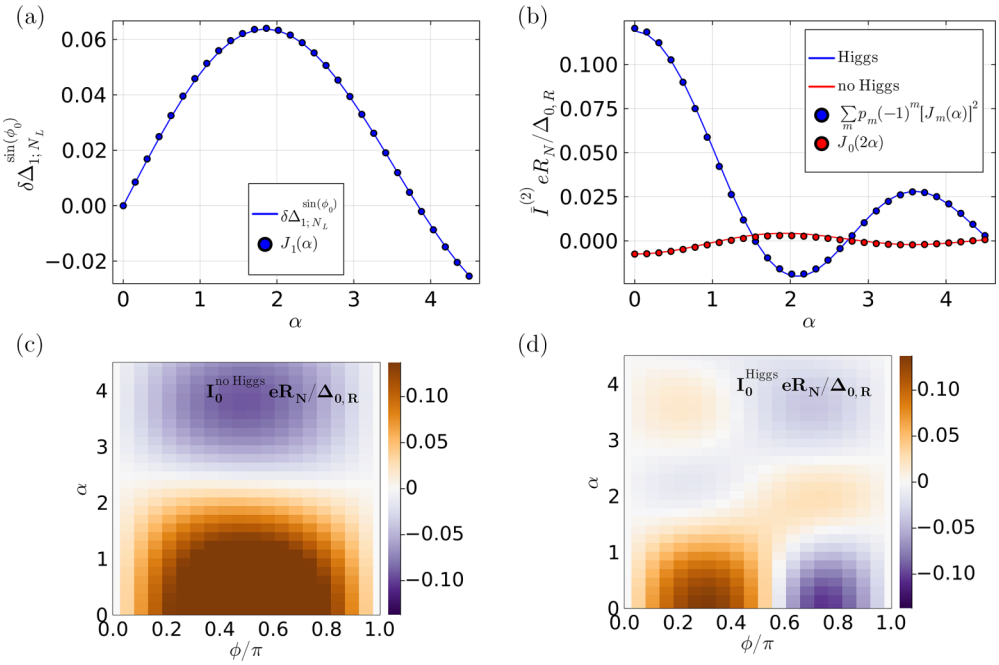

FIG. 2. (a) Numerically obtained first Floquet harmonic of the OP modulation in the left lead at the junction, $\delta\Delta_{1;j=N_L}$ [$n=1$, $j=N_L$; cf. Eq. (29)], for $N_L=18$, $N_R=5$ [47], $\mathcal{T}/\zeta=0.4$ (transparency ≈0.48 [43]), $\Gamma=0.0125\Delta_{0,R}=0.0025\zeta$, and $\omega_r\approx 2.29\Delta_{0,L}\approx 1.14\omega_{H,L}$, just over the Higgs resonance. As anticipated from Eq. (5), the dominant contribution varies as $\sin(\phi_0)$ (shown here, denoted by the subscript). The $\cos(\phi_0)$ component (not shown) is much weaker. The predicted $J_1(\alpha)$ dependence is also confirmed, as indicated by the blue circles. (b) The second-harmonic component of the CPR, $\bar{I}^{(2)}$, as a function of α. We present the normalized quantity $\bar{I}^{(2)}eR_N/\Delta_{0,R}$, where R_N is the numerically obtained normal-state resistance. For reference, in symmetric ($\Delta_{0,L}=\Delta_{0,R}=\Delta_0$) tunnel JJs $I^{(1)}$ satisfies the Ambegaokar-Baratoff result $I^{(1)}eR_N/\Delta_0=\pi/2$ [52]. In the Higgs-free case (red), obtained by retaining only the zeroth Floquet component of the OP in the self-consistency equation Eq. (26), we confirm the expected $J_0(2\alpha)$ dependence [cf. Eq. (4)]. With Higgs renormalization included (blue), $\bar{I}^{(2),\text{Higgs}}$ is much larger. It starts out positive at $\alpha=0$, in contrast to the Higgs-free case. Moreover, inspired by Eq. (6), the numerical results are well described by a fit of the form $\sum_m p_m[J_m(\alpha)]^2$, with the coefficients p_m obtained from least-squares regression. We find that $p_{m\geqslant 5}$ are negligible. (c) We show the CPR I_0 with varying α, in the absence of Higgs renormalization. Since $\bar{I}^{(2),\text{no Higgs}}$ is negligible, the CPR is not noticeably altered from $I_0\sim I^{(1)}J_0(\alpha)\sin(\phi_0)$. (d) Same as (c), but now we include the Higgs renormalization. Since $\bar{I}^{(2),\text{Higgs}}$ is large, it imparts a $\sin(2\phi_0)$ phase dependence, with the α dependence following from Eq. (6) [see also panel (b)].

A. Phase bias: Current-phase relation

We start by exploring the first proposal in Fig. 2, presenting the Higgs-renormalized CPR I_0 (dc supercurrent) in the absence of a dc voltage bias. We verify key predictions from the phenomenological analysis regarding how both the CPR and the OP depend on the radiation strength α, keeping the radiation frequency ω_r fixed. We begin by examining the Higgs-induced OP modulation, as it ultimately determines how the current depends on α. Specifically, Fig. 2(a) confirms the prediction of Eq. (5): the first Floquet component of the left order parameter at the junction, $\delta\Delta_{1;N_L}$, varies with the Josephson phase as $\sin(\phi_0)$ and scales with α as $J_1(\alpha)$. We find that the $\cos(\phi_0)$ component is negligible. Next, before addressing the full CPR, we first examine the behavior of its second-harmonic component, which varies with the Josephson phase as $\sim\sin(2\phi_0)$ [cf. Eq. (4)]. Its amplitude is calculated as $\bar{I}^{(2)}=(2/\pi)\int_0^\pi d\phi_0 I_0(\phi_0)\sin(2\phi_0)$, where I_0 is numerically obtained using Eq. (32b). Figure 2(b) shows the qualitative difference in $I^{(2)}$ with and without Higgs renormalization: in the Higgs-free case ($\bar{I}^{(2),\text{no Higgs}}$) it follows the expected $J_0(2\alpha)$ scaling [cf. Eq. (4)], is negative near $\alpha=0$, and remains small, whereas including the Higgs renormalization strongly enhances $I^{(2),\text{Higgs}}$, and crucially, makes it positive at $\alpha=0$. Note that we enforce the absence of Higgs oscillations by using a static gap, retaining only the zeroth Floquet component while self-consistently solving for the gap using Eq. (26). We reiterate that with Higgs renormalization, the second-harmonic component not only intensifies in amplitude but it also exhibits a distinct dependence on the radiation strength [compare Eqs. (4) and (6)]. Indeed, as shown in Fig. 2(b), the Higgs-renormalized second harmonic is well captured by the fit $\sum_m p_m[J_m(\alpha)]^2$, as obtained in Eq. (6). Finally, we are now able to understand the full CPR shown in Figs. 2(c) and 2(d), whose distinctive behavior in the presence of the Higgs renormalization derives from that of its second-harmonic component, $I^{(2),\text{Higgs}}$. In the Higgs-free case [Fig. 2(c)], noting that $\bar{I}^{(2),\text{no Higgs}}\ll\bar{I}^{(1)}$ for the transparencies and equilibrium gap asymmetries considered in this work, we obtain from Eq. (4) $I_0\approx\bar{I}^{(1)}\sin(\phi_0)$. Thus, the CPR maintains its typical $\sin(\phi_0)$ phase dependence, along with the associated $\sim J_0(\alpha)$ α dependence. In contrast, in the presence of Higgs renormalization [Fig. 2(d)], the CPR is strongly modified by the enhanced second harmonic, $\bar{I}^{(2),\text{Higgs}}$, with $I_0\approx\bar{I}^{(1)}\sin(\phi_0)+\bar{I}^{(2),\text{Higgs}}\sin(2\phi_0)$. This not only introduces a clear $\sin(2\phi_0)$ phase dependence, but also leads to a distinct α dependence via $\bar{I}^{(2),\text{Higgs}}$ consistent with Eq. (6). We emphasize that even if $\bar{I}^{(2),\text{no Higgs}}$ were sizable, it may be clearly distinguished from the Higgs-renormalized case

as their signs and α dependences differ [Fig. 2(b)], both of which are reflected in the full CPR. When the second harmonic is negligible, the CPR [$\sim \sin(\phi_0)$] is symmetric about $\phi_0 = \pi/2$ and remains positive for $\phi_0 \in (0, \pi)$. However, a negative (positive) second harmonic skews the CPR backward (forward). Moreover, if the second harmonic is sufficiently large, $|\bar{I}^{(2),\text{Higgs}}| > 0.5\bar{I}^{(1)}$, it can drive the CPR below zero near $\phi_0 = 0$ ($\phi_0 = \pi$).

Next, in Fig. 3 we complement the analysis in Fig. 2 by studying the dependence of the CPR and OP on ω_r and equilibrium gap asymmetry, for a fixed value of α. In Figs. 3(a) and 3(b), we plot the CPR as a function of the equilibrium gap asymmetry for two fixed values of ω_r, at a fixed radiation strength $\alpha = 2$. A clear transition appears at $\omega_r = \omega_{H,L} = 2\Delta_{0,L}$; for $\omega_r > 2\Delta_{0,L}$, the CPR dips below zero near $\phi_0 = 0$, signaling a sizable negative Higgs-induced $\bar{I}^{(2),\text{Higgs}}$ [see Fig. 2(b), which shows $\bar{I}^{(2),\text{Higgs}} < 0$ at $\alpha = 2$ when ω_r is slightly above $2\Delta_{0,L}$]. Instead, for $\omega_r < 2\Delta_{0,L}$, this negative dip disappears. The corresponding plots in the absence of Higgs renormalization, shown in Figs. 3(c) and 3(d), do not exhibit such a transition, lacking a negative dip altogether. This suggests $\bar{I}^{(2),\text{no Higgs}}$ is negligible. In Fig. 3(e), we see the resonant enhancement of the OP at $\omega_r = \omega_{H,L}$, as predicted by Eq. (5). Recall from the same equation that the harmonics $\delta\Delta_m$ decay as $J_m(\alpha)$. No signatures of higher-order resonances at $m\omega_r = \omega_{H,L}$ are observed for $\alpha = 2$. In Figs. 3(f) and 3(g), we show the amplitudes of the second-harmonic component with and without Higgs renormalization, respectively. The former is negative, and shows a resonant enhancement at $\omega_r = \omega_{H,L}$, while the latter is positive [see Fig. 2(b)].

B. Voltage bias: Shapiro steps

Let us now discuss the signature of the Higgs mode in the Shapiro steps that appear as a consequence of the phase locking between the microwave field and the applied dc voltage bias. In Fig. 4, to clarify the impact of Higgs renormalization, we proceed by examining the OP and the current harmonics I_{ω_J} and $I_{2\omega_J}$ in dc voltage-biased JJs in the absence of radiation, comparing results with and without the Higgs renormalization. We find that I_{ω_J} exhibits no significant qualitative changes in the presence of Higgs renormalization [compare Figs. 4(a) and 4(b)]. The Higgs oscillations mainly appear as a nonequilibrium OP component oscillating at frequency ω_J, which is shown in Figs. 4(c) and 4(d). Its amplitude peaks at the Higgs resonance, $\omega_J = \omega_{H,L}$. In highly asymmetric junctions, these Higgs oscillations result in a pronounced peak in the second-harmonic Josephson current $I^{\text{Higgs}}_{2\omega_J}$ as the bias voltage is tuned across the Higgs resonance [Fig. 4(f)]. By contrast, without Higgs oscillations, $I^{\text{no Higgs}}_{2\omega_J}$ is much smaller and no such peak arises [Fig. 4(e)].

Now, armed with an understanding of the effect of the Higgs renormalization on the ac Josephson current harmonics, we are ready to look at how these manifest in the SSs in irradiated dc voltage-biased JJs in Figs. 5 and 6. Specifically, we focus on two SSs, SS^1_1 in Fig. 5 and SS^2_1 in Fig. 6, which require $\omega_J = \omega_r$ and $2\omega_J = \omega_r$, respectively. Before turning to the role of Higgs renormalization, we first consider the trivial case where it is absent. Even for the high transparencies ($\approx$0.48) studied here, the $2\omega_J$ current arising from higher-order Josephson processes remains much smaller than the conventional ω_J current given by Eq. (9). In fact, as shown in Figs. 4(c) and 4(d), a large equilibrium gap asymmetry ($\Delta_{0,L} \ll \Delta_{0,R}$ without loss of generality) aids the suppression of the $2\omega_J$ current. As such, we expect the current to be described by Eq. (9), containing only the ω_J current, I_{ω_J}. Furthermore, while the amplitude of I_{ω_J} is expected to be dependent on both ω_J and ω_r [$I_{\omega_J}(\omega_J, \omega_r)$], for small ω_J, along with radiation of low intensity (low α) and low frequency ω_r, the frequency dependence of I_{ω_J} may be neglected and replaced with its zero-frequency value. As derived in Eq. (10), this yields $SS^1_1 = 2I_{\omega_J}J_{-1}(\alpha)$ with the distinctive $J_{-1}(\alpha)$ profile [77,78]. For the values of α and ω_r considered in this work, as shown in Fig. 5(b), we find that this is indeed the case, with no significant differences from the $J_{-1}(\alpha)$ profile. Turning to SS^2_1, we recall from Eq. (13) that it is governed solely by $I_{2\omega_J}$. As noted above, $I^{\text{no Higgs}}_{2\omega_J}$ is much smaller than $I^{\text{no Higgs}}_{\omega_J}$ in the absence of Higgs renormalization. Consequently, $SS^2_{1,\text{no Higgs}}$ has a much smaller magnitude compared to $SS^1_{1,\text{no Higgs}}$, which depends on both $I^{\text{no Higgs}}_{\omega_J}$ and $I^{\text{no Higgs}}_{2\omega_J}$ [Eq. (10)]. This difference is clearly visible when comparing their amplitudes in Figs. 5(b) and 6(b), which reveal that the crests of $SS^2_{1,\text{no Higgs}}$ are nearly two orders of magnitudes smaller than those of $SS^1_{1,\text{no Higgs}}$.

Now, we turn to the case with Higgs renormalization. We begin with $SS^1_{1,\text{Higgs}}$, shown in Fig. 5(a), where it is plotted as a function of α for several bias voltages ω_J ranging from below the Higgs resonance ($\omega_J \lesssim \omega_{H,L}$) to well above it ($\omega_J \gg \omega_{H,L}$). Recall that $SS^1_{1,\text{Higgs}}$ depends on a combination of $J_{-1}(\alpha)$ and $J_{-2}(2\alpha)$, weighted by $I^{\text{Higgs}}_{\omega_J}$ and $I^{\text{Higgs}}_{2\omega_J}$, respectively [cf. Eq. (16)]. At the resonance $\omega_J \approx \omega_{H,L}$, the strong Higgs-renormalized contribution to $I_{2\omega_J}$ amplifies the $J_{-2}(2\alpha)$ term, producing clear deviations from the $J_{-1}(\alpha)$ behavior observed in the absence of Higgs renormalization [cf. Fig. 4(d)]. Even more striking is the behavior of SS^2_1, which according to Eq. (16) depends exclusively on $I^{\text{Higgs}}_{2\omega_J}$. Since $I^{\text{Higgs}}_{2\omega_J}$ becomes comparable in size to $I^{\text{Higgs}}_{\omega_J}$ near the resonance, $SS^2_{1,\text{Higgs}}$ attains a magnitude similar to $SS^1_{1,\text{Higgs}}$, as evident in Figs. 5(a) and 6(a). This provides a clear fingerprint of Higgs renormalization in conventional JJs, as no other mechanism can generate such a pronounced increase in the $2\omega_J$ current.

Now we comment on the applicability of the AA introduced earlier. As shown in Figs. 5(c) and 6(a), we find that for small $\omega_r < \Delta_{0,R}$, our numerical results are matched by the AA [Eqs. (15) and (16), respectively]. Specifically, on starting with the numerically obtained coefficients $I_{\omega_J} = \Im(I_{20} - I_{-20})$ and $I_{2\omega_J} = \Im(I_{40} - I_{-40})$ at $\alpha = 0$, which represent the amplitudes of the $\sin(\omega_J t)$ and $\sin(2\omega_J t)$ currents in the absence of radiation, the numerically obtained SS^1_1 and SS^2_1 mirror Eqs. (15) and (16), respectively [76]. For large values of ω_r comparable to or larger than $\Delta_{0,R}$, we find significant deviations from the AA predictions. The validity of the AA is primarily limited by electronic retardation processes, which imbibe the amplitudes I_{ω_J} and $I_{2\omega_J}$ with frequency dependence [77,78]. A detailed account of this argument may be found in Chap. 11 of Refs. [42,79]. In particular, a leading-order perturbative (in the tunnel coupling $\mathcal{T}$) calculation reveals resonances at frequency $\Delta_{0,L/R}$ or $\Delta_{0,L} \pm \Delta_{0,R}$, corresponding to

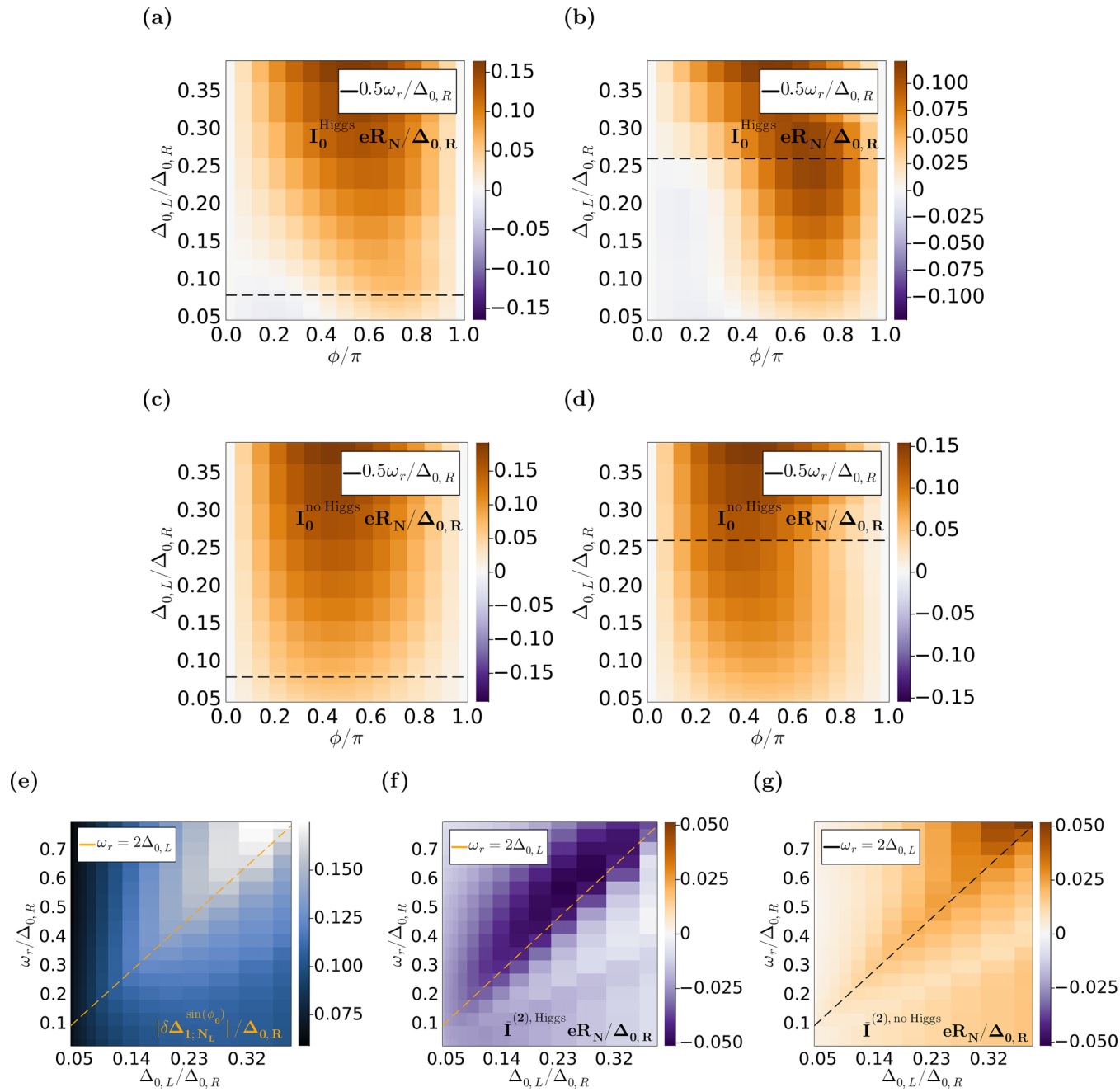

FIG. 3. (a)–(d) Numerically obtained CPR (I_0) at $\alpha = 2$, in a system with $N_L = 18, N_R = 5$ [47], $\mathcal{T}/\zeta = 0.4$ (transparency ≈0.48 [43]), and $\Gamma = 0.0125\Delta_{0,R} = 0.0025\zeta$. We present the normalized quantity $I_0 eR_N/\Delta_{0,R}$, where R_N is the numerically obtained normal-state resistance. (a), (b) CPR as a function of the equilibrium gap asymmetry $\Delta_{0,L}/\Delta_{0,R}$. Each panel considers a different ω_r. The black dashed line marks the point $0.5\omega_r/\Delta_{0,R} = \Delta_{0,L}/\Delta_{0,R}$, corresponding to the resonance condition $\omega_r = 2\Delta_{0,L}$. The Higgs renormalization weakens as $2\Delta_{0,L}$ exceeds ω_r, restoring the conventional $\sim \sin(\phi_0)$ behavior. In contrast, when $2\Delta_{0,L}$ moves below ω_r, the CPR develops a negative dip near $\phi_0 = 0$, originating from the Higgs-induced term $\bar{I}^{(2),\mathrm{Higgs}} \sin(2\phi_0)$, with $\bar{I}^{(2),\mathrm{Higgs}} < 0$ [see Fig. 2(b) for the sign at $\alpha = 2$]. Panels (c) and (d) show the corresponding results without Higgs renormalization. We do not find any negative dips in I_0. (e) The component of the OP varying as $\sin(\phi_0)$ [the $\cos(\phi_0)$ component is negligible] in the left lead at the junction ($x = N_L$), which is peaked at the Higgs resonance $\omega_r = 2\Delta_{0,L}$. This resonance is marked by a dashed line in all remaining panels. (f) Second harmonic $\bar{I}^{(2),\mathrm{Higgs}}$ as a function of ω_r and $\Delta_{0,L}/\Delta_{0,R}$, showing the Higgs resonance. The Higgs-free counterpart in panel (g) exhibits the opposite sign [see Fig. 2(b)]. In this case, the peak at $\omega_r = 2\Delta_{0,L}$ corresponds to the pair-breaking threshold.

resonant excitation of quasiparticles between the singular gap edges of the two SC leads. Since the dominant contribution to the current typically arises from the exchange of only the few lowest harmonics of ω_J and ω_r, for small values of ω_r and ω_J, the components I_{ω_J} and $I_{2\omega_J}$ are probed only near zero frequency, and their frequency dependence can therefore be neglected. However, for ω_J and ω_r comparable to the resonant frequencies mentioned above, or for larger transparency and

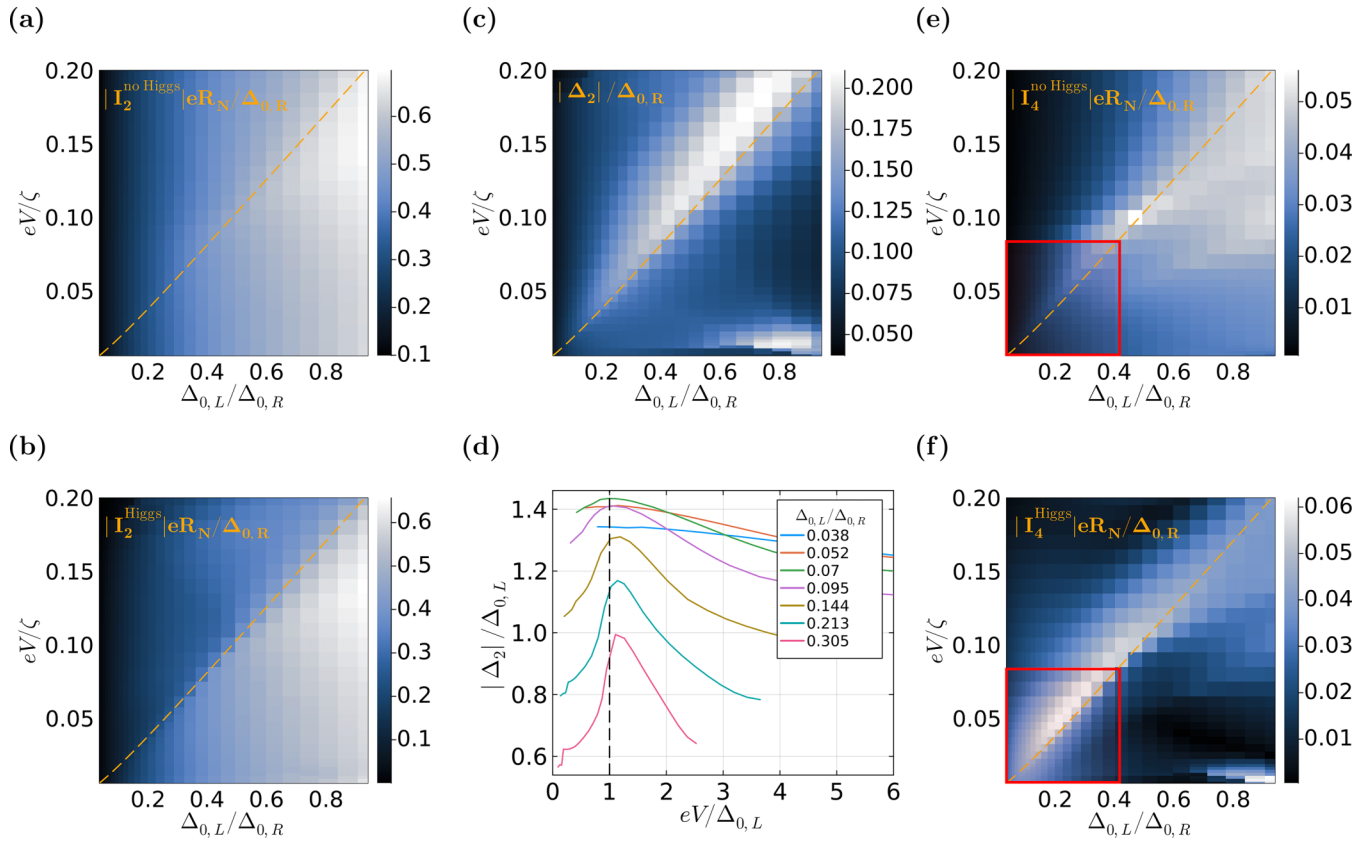

FIG. 4. Numerically obtained current harmonics without radiation, in a system with $N_L = 18$, $N_R = 5$ [47], $\mathcal{T}/\zeta = 0.4$ (transparency $\approx$0.48 [43]), and $\Gamma = 0.0125\Delta_{0,R} = 0.0025\zeta$. Panels (a) and (b) show I_{ω_J} without ($I_2^{\text{no Higgs}}$) and with (I_2^{Higgs}) Higgs oscillations, respectively; they exhibit no significant qualitative differences. The orange diagonal dashed line marks the Higgs resonance, 2 eV $= 2\Delta_{0,\text{L}}$, in all the heat maps. (c) Δ_2 (OP component oscillating at frequency ω_J), normalized by $\Delta_{0,R}$, which exhibits a peak at the Higgs resonance (orange dashed line). The small offset from the resonance likely originates from a local enhancement of $\Delta_{0,L}$ near the junction barrier due to the proximity effect. (d) Cuts of Δ_2, normalized by $\Delta_{0,L}$, as a function of eV for various values of $\Delta_{0,L}$. It is peaked at the Higgs resonance (vertical dashed line), with the peak achieving its maximum value for $\Delta_{0,L}/\Delta_{0,R} \approx 0.07$. Panels (e) and (f) show $|I_{2\omega_J}|$, in the absence ($I_4^{\text{no Higgs}}$) and presence (I_4^{Higgs}) of Higgs renormalization, respectively. In the absence of Higgs renormalization (e), only a small $2\omega_J$ current appears, attributable to higher-order Josephson effect. In contrast, with Higgs renormalization (f), a pronounced peak emerges at the Higgs resonance (orange dashed line), particularly in the highly asymmetric regime where $\Delta_{0,L} \ll \Delta_{0,R}$ (bottom-left corner, highlighted by the red box). In the same regime (once again, highlighted by a red box), panel (e) shows that $I_4^{\text{no Higgs}}$ remains much smaller.

α when higher harmonics of ω_J and ω_r also participate via higher-order tunneling processes, this frequency dependence may no longer be neglected. It introduces an explicit dependence on the harmonic number in the current amplitudes, which modifies the Bessel function amplitudes derived within the AA.

V. DISCUSSION AND CONCLUSIONS

In this work, we demonstrate that the Higgs mode can be excited and detected in highly asymmetric, high-transparency JJs under microwave irradiation. We propose two approaches: (i) measuring the second harmonic of the current-phase relation, whose Higgs-renormalized dependence on radiation strength deviates strongly from the Higgs-free case, and (ii) applying a dc voltage bias, where the Higgs-renormalized second-harmonic ac Josephson current can be extracted from Shapiro step measurements.

We note that a recent work by Vallet and Cayssol [21] had explored a similar, yet different scenario, wherein the Higgs mode is excited by irradiating the *bulk* of the SC leads by a *uniform* THz electric field. This corresponds to the SC leads being subjected to a uniform bulk vector potential **A** oscillating at frequency ω_r. This is not equivalent to our case, where we assume that the radiation induces a time-dependent potential difference between the two SC leads V_{ac} [41–46], with the drop restricted to the barrier region [24]. Indeed, Ref. [21] considered an OP oscillating as $\Delta(t) = \Delta_0 + \delta\Delta_{\text{VC}}(t)$, where $\delta\Delta_{\text{VC}}(t) = 2\Re(\Delta_2 e^{-i2\omega_r t})$, arising from the second-order coupling of the OP to the oscillating bulk vector potential [17], which differs from our results as the spectrum of $\delta\Delta_{\text{VC}}$ does not contain: (i) any multiples of ω_J, and (ii) the first harmonic of the radiation frequency ω_r. (i) follows from the fact that Ref. [21] only considered tunnel JJs; oscillations in $\delta\Delta_{\text{VC}}(t)$ at frequency ω_J are $\mathcal{O}(\mathcal{T}^2)$ and they contribute to the current only at $\mathcal{O}(\mathcal{T}^4)$, while the leading-order Josephson current is $\mathcal{O}(\mathcal{T}^2)$. In our case, by arguments of gauge invariance, it is clear that the OP must respond to the gauge-invariant Josephson phase given by Eq. (2) and thus, $\delta\Delta(t)$ is bound to contain ω_J, as well as *all* harmonics of ω_r (not just the even

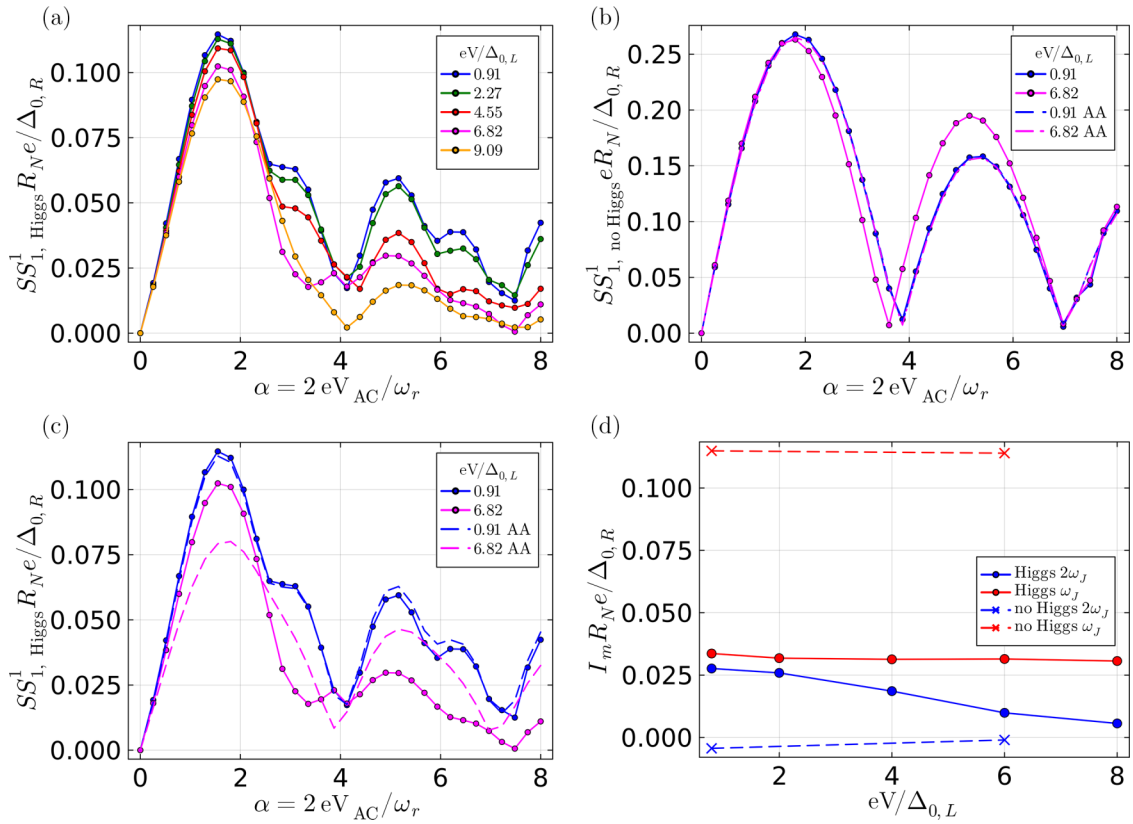

FIG. 5. Numerically calculated Shapiro step height SS^1_1 [Eq. (28)], in a system with $N_L = 18$, $N_R = 5$ [47], $\mathcal{T}/\zeta = 0.4$ (corresponding to transparency ≈0.48 [43]), $\Delta_{0,L} = 0.045\Delta_{0,R} = 0.0088\zeta$, and $\Gamma = 0.0125\Delta_{0,R} = 0.0025\zeta$. We plot the normalized quantity $SS^1_1 R_N e/\Delta_{0,R}$ as a function of the radiation strength α, for various values of the dc voltage eV sweeping across and beyond the Higgs resonance $\text{eV} = \Delta_{0,\text{L}}$. We show it in (a) the presence and (b) the absence of Higgs renormalization. In its presence, $SS^1_{1,\text{Higgs}}$ noticeably deviates from the $J_{-1}(\alpha)$ profile, evident most immediately from the changes in the location and magnitudes of the nodes/dips as a function of α. On the other hand, in the absence of Higgs renormalization [panel (b)], while $SS^1_{1,\text{no Higgs}}$ is still altered by the presence of $I_{2\omega_J}$ arising solely from higher-order Josephson processes [cf. Eq. (12)], for the chosen transparency this contribution is insufficient to generate noticeable deviations from the expected $\sim J_{-1}(\alpha)$ dependence. Panel (c) compares the exact numerical results from (a) (solid lines with markers) with the AA of Eq. (15) (dashed lines). The AA is evaluated using the numerically obtained currents [Eq. (27b)] with $I_{\omega_J} = \Im(I_{20} - I_{-20})$ and $I_{2\omega_J} = \Im(I_{40} - I_{-40})$. Our goal is to test whether the α dependence of S^1_1 (but not that on the dc voltage) can be captured by the AA [Eq. (12)]. For small ω_J and ω_r, the AA agrees well with the numerical results, reproducing the Higgs-induced deviations from the $J_{-1}(\alpha)$ profile shown in (b). Finally, panel (d) presents the amplitudes of the ω_J and $2\omega_J$ currents, with $I_{\omega_J} = I_2$ (red) and $I_{2\omega_J} = I_4$ (blue), both with and without Higgs renormalization, as functions of the bias voltage. I_4 decreases away from the resonance.

ones, or just $2\omega_r$) in its spectrum. Consequently, Ref. [21] did not obtain a Higgs-induced correction to SS^1_1 at $\omega_J = \omega_r$, nor did they obtain SS^2_1 at $2\omega_J = \omega_r$, both of which are present in our results shown in Figs. 5 and 6. Instead, they only obtained SS^1_2 at $\omega_J = 2\omega_R$. Similarly, in the phase-biased case, the resonance at $\omega_r = 2\Delta_{0,L}$ in the second harmonic of the CPR was absent when $\delta\Delta$ lacks a component oscillating at ω_r. Instead, the leading resonance appeared at $2\omega_r = 2\Delta_{0,L}$. We remark that these differences result from the two physically distinct excitation processes considered by them and this work.

Finally, we comment on the practical realization of our proposal. Since our aim is to realize highly asymmetric Josephson junctions using conventional s-wave superconductors, Al-based junctions appear to be the most promising choice, owing to their small gap (≈45 GHz in the bulk limit) and the flexibility of tuning the equilibrium gap by varying the thickness [80–86]. The asymmetry can be further tuned by raising the temperature, since the smaller gap decreases more rapidly with increasing temperature. As shown in Fig. 1, we require long junctions with leads of lengths larger than the corresponding superconducting coherence lengths, along with high transparencies. We note that a compromise can be achieved by increasing the equilibrium gap asymmetry, which in turn allows the use of smaller transparencies. According to our numerical calculations (Ref. [24], which considered two- and three-dimensional models, as well as this work), which are limited to a maximum equilibrium gap asymmetry $\Delta_{0,L}/\Delta_{0,R} \approx 0.05 - 0.1$ due to computational bottlenecks (the Higgs resonance condition requires $\text{eV} = \Delta_{0,\text{L}}$, and smaller values of eV necessitate more Floquet modes), in order to achieve $I_{2\omega_J} \sim I_{\omega_J}$ we require transparencies $\gtrsim$0.4. Nevertheless, even at lower transparencies or lower asymmetry, when $I_{2\omega_J} < I_{\omega_J}$, the presence of Higgs renormalization can still be inferred from the resonant amplification of its signatures on tuning the voltage bias across the Higgs resonance condition $\omega_J = \omega_H$.

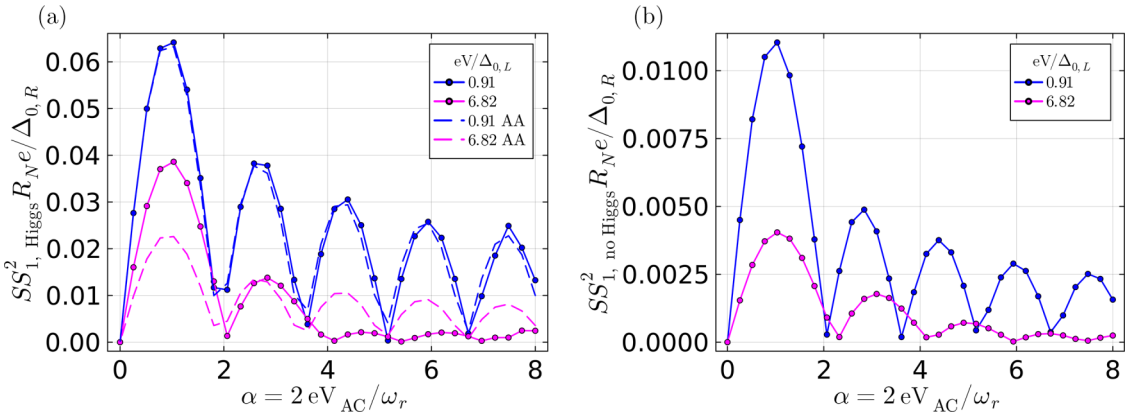

FIG. 6. (a) Same as Fig. 5(c) (including the parameters, except for ω_r), but we show SS_1^2, where $2\omega_J = \omega_r$. $SS^2_{1,\text{Higgs}}$, which arises from the Higgs-enhanced $I^{\text{Higgs}}_{2\omega_J}$, is approximately of the same magnitude as $SS^1_{1,\text{Higgs}}$ in Fig. 5 as $I^{\text{Higgs}}_{2\omega_J} \sim I^{\text{Higgs}}_{\omega_J}$. Similar to Fig. 5(c), we overlay the AA results given by Eq. (16) using dashed lines. These match the numerical results only for small ω_J and ω_r. (b) Same as (a), but we show the data in the absence of Higgs renormalization. Notice that now $SS^2_{1,\text{no Higgs}}$ is about an order of magnitude smaller than its Higgs renormalized counterpart in (a). For the chosen value of transparency ≈0.48, the higher-order Josephson current $I^{\text{no Higgs}}_{2\omega_J}$ is far from sufficient to match the Higgs-renormalized $I^{\text{Higgs}}_{2\omega_J}$ [cf. Eq. (13). See also Fig. 5(d)].

ACKNOWLEDGMENTS

This work was supported by the Würzburg-Dresden Cluster of Excellence ct.qmat, EXC2147, Project ID No. 390858490, and the DFG (SFB 1170), Project ID No. 258499086. The authors gratefully acknowledge the scientific support and HPC resources provided by the Erlangen National High Performance Computing Center (NHR@FAU) of the Friedrich-Alexander-Universität Erlangen-Nürnberg (FAU) under the NHR Project No. b169cb. NHR funding is provided by federal and Bavarian state authorities. NHR@FAU hardware is partially funded by the German Research Foundation (DFG) Grant No. 440719683.

DATA AVAILABILITY

The data that support the findings of this article are not publicly available upon publication because it is not technically feasible and/or the cost of preparing, depositing, and hosting the data would be prohibitive within the terms of this research project. The data are available from the authors upon reasonable request.

APPENDIX A: PHENOMENOLOGICAL MODEL FOR HIGGS EXCITEMENT IN JOSEPHSON JUNCTIONS

In this Appendix, we show how the Higgs mode is excited in a JJ using a toy model for the superconducting condensates of two tunnel coupled superconducting leads. In this simple analysis, we only look at a linear response calculation at the leading order in the Josephson coupling between the condensates of the two SCs. We thus start with the Euclidean action describing the effective field theory of the condensates, represented by a complex scalar field Ψ minimally coupled [87] to a scalar potential field V. An equivalent analysis may be performed in the Keldysh space for the nonlinear response. The action is given by

$$S = \int_{\tau,\mathbf{r}} \sum_{j=L/R} \Big[|(\partial_\tau + i2\ \mathrm{eV_j}(\tau))\Psi_j|^2 + c^2|\nabla\Psi_j|^2 + \frac{a_j}{2}|\Psi_j|^2 + \frac{u}{4}|\Psi_j|^4 \Big] - \int_\tau J(\bar{\Psi}_{L,x=0}\Psi_{R,x=0} + \bar{\Psi}_{L,x=0}\Psi_{R,x=0}). \tag{A1}$$

Here $V_L = V(\tau)$ and $V_R = 0$, without loss of generality, capture the potential difference, $a_j \sim (T - T_{C,j})/T_{C,j}$ ($T_{C,j}$ is the critical temperature of the jth lead) in the superconducting phase, and J is the Josephson coupling. Note that in Euclidean space, the minimally coupled scalar potential, transforming like the timelike component of the electromagnetic four-potential, gets an additional factor of i as well [87].

We use the ansatz $\Psi_j = (\Delta_{0,j} + h_j)e^{-i\vartheta_j}$ to separate the mean gap amplitudes $\Delta_{0,j} = \sqrt{-|a_j|/u}\Theta(-a_j)$ of the isolated condensates, the Higgs fields h_j, and the complex phase factor $e^{-i\vartheta_j}$. The relevant terms in the resulting action is obtained as

$$S = \int_{\tau,\mathbf{r}} \sum_{j=L/R} \Big[(\partial_\tau h_j)^2 + c^2(\nabla h_j)^2 + \frac{|a_j|}{2}|h_j|^2 + \Delta_{0,j}^2[(\partial_\tau\vartheta_j - 2\ \mathrm{eV}_j(\tau))^2 + c^2(\nabla\vartheta_j)^2] \Big] - \int_\tau 2J\Delta_{0,L}h_{R,x=0}\cos(\vartheta_{L,x=0}(\tau) - \vartheta_{R,x=0}(\tau)) - \int_\tau 2Jh_{L,x=0}\Delta_{0,R}\cos(\vartheta_{L,x=0}(\tau) - \vartheta_{R,x=0}(\tau)). \tag{A2}$$

Here, $|a_j|/2$ is the mass of h_j. The phase-field fluctuations are massive, and thus the phase settles into its mean-field value, satisfying the Josephson relation $\partial_\tau\vartheta_j = 2eV_j(\tau)$. Defining

$X(\tau) = 2J\Delta_{0,R}\cos(\vartheta_{L,x=0} - \vartheta_{R,x=0})$,

$$\langle h_{L,i\omega_n,\mathbf{k}}\rangle = \frac{X_{i\omega_n}}{\omega_n^2 + c^2\mathbf{k}^2 + \frac{|a_L|}{2}}. \tag{A3}$$

On analytically continuing to real time

$$\langle h_{L,\omega,\mathbf{k}}\rangle = \frac{X_\omega}{-(\omega + i0)^2 + c^2\mathbf{k}^2 + \frac{|a_L|}{2}}, \tag{A4}$$

where X_ω is the Fourier transform of $\cos(\vartheta_{L,x=0}(t) - \vartheta_{R,x=0}(t))$. Note that along with $\tau \to it$, we also require $V \to -iV$ [87,88].

For a dc voltage bias, the Josephson phase $\phi = \vartheta_L - \vartheta_R$ satisfies $\partial_\tau\phi = 2e(V_L - V_R) = 2$ eV. Now, we assume without loss of generality that $a_L \ll a_R$ (corresponding to $\Delta_{0,L} \ll \Delta_{0,R}$, which suppresses the Higgs field in the R condensate). Hence,

$$S = \int_{\tau,\mathbf{r}} \sum_{j=L/R} \left[(\partial_\tau h_j)^2 + c^2(\nabla h_j)^2 + \frac{|a_j|}{2}h_j^2\right] - \int_\tau 2J(\Delta_{0,L}h_{R,x=0} + h_{L,x=0}\Delta_{0,R})\cos(2\,\mathrm{eV}\tau). \tag{A5}$$

Clearly, we see that the Higgs field responds at frequency 2 eV, and the response is peaked at the Higgs mass 2 eV $= |a_L|/2$. Thus, we see that the potential difference V provides a dynamic excitation to the Higgs field at frequency 2 eV, essentially arising from the interference of the two OPs whose phases differ by 2 eVt. This is embodied in the tunneling action $S_T = -\int_\tau 2Jh_{L,x=0}\Delta_{0,R}\cos(2\,\mathrm{eV}\tau)$, which in Minkowski space becomes $S_T = -i\int_t 2Jh_{L,x=0}\Delta_{0,R}\cos(2\ \mathrm{eV}t)$. Note that the analysis of the regime 2 eV $> |a_L|/2$ requires an account of the damping of the Higgs mode, which we have neglected in this toy model.

APPENDIX B: PSEUDO-FLOQUET DECOMPOSITION

Here we discuss the representation used in Eq. (23), which is not the usual Floquet decomposition. This is because, in general, there is no periodicity when $\omega_J/2$ and ω_r are incommensurate. We do, however, recover the periodicity for $\omega_r = 0$ (or $\omega_J = 0$). In this case, we can split the frequency integral into intervals of length equaling the Floquet frequency $\Omega = \omega_J/2$ as the periodic perturbation always scatters between two frequencies separated by Ω and never within a single interval. A two-point function which is periodic in the average argument, $G(t+T, t'+T) = G(t,t') \iff G(t_{\mathrm{av}} + T, \delta t) = G(t_{\mathrm{av}}, \delta t)$ where $t_{\mathrm{av}} = (t+t')/2$, admits the usual Floquet expansion:

$$G(t,t') = \sum_{m,n}\int_0^\Omega \frac{d\omega}{2\pi}\overbrace{G(\omega + m\Omega, \omega + n\Omega)}^{G_{mn}(\omega)} \times e^{-i(\omega+m\Omega)t + i(\omega+n\Omega)t'}, \tag{B1}$$

where $G_{mn}(\omega)$ satisfies

$$G((\omega+\Omega) + m\Omega, (\omega+\Omega) + n\Omega) = G_{(m+1)(n+1)}(\omega). \tag{B2}$$

In this case, the pseudo-Floquet one given by Eq. (23) and the usual Floquet one in Eq. (B1) are equivalent:

$$\begin{aligned} G(t,t') &= \sum_m \int_{-\infty}^\infty \frac{d\omega}{2\pi} G(\omega + m\Omega, \omega)e^{-i(\omega+m\Omega)t + i\omega t'} \\ &= \sum_{m,k}\int_0^\Omega \frac{d\omega}{2\pi} G_{m0}(\omega + k\Omega)e^{-i(\omega+k\Omega+m\Omega)t + i(\omega+k\Omega)t'} \\ &= \sum_{m,k}\int_0^\Omega \frac{d\omega}{2\pi} G_{(m+k)(k)}(\omega)e^{-i(\omega+(m+k)\Omega)t + i(\omega+k\Omega)t'} \\ &\xrightarrow[k\to n]{m+k\to m} \sum_{m,n}\int_0^\Omega \frac{d\omega}{2\pi} G_{mn}(\omega)e^{-i(\omega+m\Omega)t + i(\omega+n\Omega)t'}. \end{aligned} \tag{B4}$$

[1] P. W. Higgs, Broken symmetries and the masses of gauge bosons, Phys. Rev. Lett. **13**, 508 (1964).

[2] P. B. Littlewood and C. M. Varma, Amplitude collective modes in superconductors and their coupling to charge-density waves, Phys. Rev. B **26**, 4883 (1982).

[3] C. Varma, Higgs boson in superconductors, J. Low. Temp. Phys. **126**, 901 (2002).

[4] D. Pekker and C. Varma, Amplitude/Higgs modes in condensed matter physics, Annu. Rev. Condens. Matter Phys. **6**, 269 (2015).

[5] R. Shimano and N. Tsuji, Higgs mode in superconductors, Annu. Rev. Condens. Matter Phys. **11**, 103 (2020).

[6] R. Matsunaga, R. Shimano, Nonequilibrium BCS state dynamics induced by intense terahertz pulses in a superconducting NbN film, Phys. Rev. Lett. **109**, 187002 (2012).

[7] R. Matsunaga, Y. I. Hamada, K. Makise, Y. Uzawa, H. Terai, Z. Wang, and R. Shimano, Higgs amplitude mode in the BCS superconductors $Nb_{1-x}Ti_xN$ induced by terahertz pulse excitation, Phys. Rev. Lett. **111**, 057002 (2013).

[8] M. Beck, I. Rousseau, M. Klammer, P. Leiderer, M. Mittendorff, S. Winnerl, M. Helm, G. N. Gol'tsman, and J. Demsar, Transient increase of the energy gap of superconducting NbN thin films excited by resonant narrow-band terahertz pulses, Phys. Rev. Lett. **110**, 267003 (2013).

[9] R. Matsunaga, N. Tsuji, H. Fujita, A. Sugioka, K. Makise, Y. Uzawa, H. Terai, Z. Wang, H. Aoki, and R. Shimano, Light-induced collective pseudospin precession resonating with Higgs mode in a superconductor, Science **345**, 1145 (2014).

[10] R. Matsunaga, N. Tsuji, K. Makise, H. Terai, H. Aoki, and R. Shimano, Polarization-resolved terahertz third-harmonic generation in a single-crystal superconductor NbN: Dominance of the Higgs mode beyond the BCS approximation, Phys. Rev. B **96**, 020505(R) (2017).

[11] K. Katsumi, N. Tsuji, Y. I. Hamada, R. Matsunaga, J. Schneeloch, R. D. Zhong, G. D. Gu, H. Aoki, Y. Gallais,

and R. Shimano, Higgs mode in the $d-$wave superconductor $Bi_2Sr_2CaCu_2O_{8+x}$ driven by an intense terahertz pulse, Phys. Rev. Lett. **120**, 117001 (2018).

[12] P. W. Anderson, Coherent excited states in the theory of superconductivity: Gauge invariance and the Meissner effect, Phys. Rev. **110**, 827 (1958).

[13] D. Sherman, U. S. Pracht, B. Gorshunov, S. Poran, J. Jesudasan, M. Chand, P. Raychaudhuri, M. Swanson, N. Trivedi, A. Auerbach, *et al.*, The Higgs mode in disordered superconductors close to a quantum phase transition, Nat. Phys. **11**, 188 (2015).

[14] H. Chu, M.-J. Kim, K. Katsumi, S. Kovalev, R. D. Dawson, L. Schwarz, N. Yoshikawa, G. Kim, D. Putzky, Z. Z. Li, *et al.*, Phase-resolved Higgs response in superconducting cuprates, Nat. Commun. **11**, 1793 (2020).

[15] C. Vaswani, J. Kang, M. Mootz, L. Luo, X. Yang, C. Sundahl, D. Cheng, C. Huang, R. H. Kim, Z. Liu, *et al.*, Light quantum control of persisting Higgs modes in iron-based superconductors, Nat. Commun. **12**, 258 (2021).

[16] M. A. Silaev, R. Ojajärvi, and T. T. Heikkilä, Spin and charge currents driven by the Higgs mode in high-field superconductors, Phys. Rev. Res. **2**, 033416 (2020).

[17] G. Tang, W. Belzig, U. Zülicke, and C. Bruder, Signatures of the Higgs mode in transport through a normal-metal–superconductor junction, Phys. Rev. Res. **2**, 022068(R) (2020).

[18] P. Vallet and J. Cayssol, Higgs amplitude mode in ballistic superconducting hybrid junctions, Phys. Rev. B **108**, 094515 (2023).

[19] V. Plastovets, A. S. Mel'nikov, and A. I. Buzdin, Collisionless dynamics of the superconducting gap excited by a spin-splitting field, Phys. Rev. B **108**, 104507 (2023).

[20] M. Heckschen and B. Sothmann, Pair-amplitude dynamics in strongly coupled superconductor–quantum dot hybrids, Phys. Rev. B **105**, 045420 (2022).

[21] P. Vallet and J. Cayssol, Anderson-Higgs amplitude mode in Josephson junctions, Phys. Rev. B **110**, 024517 (2024).

[22] T. Kuhn, B. Sothmann, and J. Cayao, Floquet engineering Higgs dynamics in time-periodic superconductors, Phys. Rev. B **109**, 134517 (2024).

[23] P. A. Lee and J. F. Steiner, Detection of collective modes in unconventional superconductors using tunneling spectroscopy, Phys. Rev. B **108**, 174503 (2023).

[24] A. Lahiri, S.-J. Choi, and B. Trauzettel, AC Josephson signatures of the superconducting Higgs mode, Phys. Rev. B **112**, 094516 (2025).

[25] B. D. Josephson, Possible new effects in superconductive, Phys. Lett. **1**, 251 (1962).

[26] D. J. Scalapino, Pair tunneling as a probe of fluctuations in superconductors, Phys. Rev. Lett. **24**, 1052 (1970).

[27] In time-reversal symmetric single-band s-wave SCs, the $2\omega_J$ component is smaller than the ω_J component, unless we have ferromagnetic components, spin-orbit interaction in the presence of a magnetic field, d- and p-wave SCs, and multiband SCs [28–39].

[28] H. Sellier, C. Baraduc, F. Lefloch, and R. Calemczuk, Half-integer Shapiro steps at the $0-\pi$ crossover of a ferromagnetic Josephson junction, Phys. Rev. Lett. **92**, 257005 (2004).

[29] H. Sickinger, A. Lipman, M. Weides, R. G. Mints, H. Kohlstedt, D. Koelle, R. Kleiner, and E. Goldobin, Experimental evidence of a ϕ Josephson junction, Phys. Rev. Lett. **109**, 107002 (2012).

[30] E. Goldobin, D. Koelle, R. Kleiner, and A. Buzdin, Josephson junctions with second harmonic in the current-phase relation: Properties of ϕ junctions, Phys. Rev. B **76**, 224523 (2007).

[31] S. M. Frolov, D. J. Van Harlingen, V. V. Bolginov, V. A. Oboznov, and V. V. Ryazanov, Josephson interferometry and Shapiro step measurements of superconductor-ferromagnet-superconductor $0-\pi$ junctions, Phys. Rev. B **74**, 020503(R) (2006).

[32] F. Li, L. Wu, L. Chen, S. Zhang, W. Peng, and Z. Wang, Measurement of the intrinsic higher harmonic current-phase relation in NbN/NiCu/NbN Josephson junctions, Phys. Rev. B **99**, 100506 (R) (2019).

[33] T. Yokoyama, M. Eto, and Y. V. Nazarov, Anomalous Josephson effect induced by spin-orbit interaction and Zeeman effect in semiconductor nanowires, Phys. Rev. B **89**, 195407 (2014).

[34] Y. Tanaka and S. Kashiwaya, Theory of Josephson effects in anisotropic superconductors, Phys. Rev. B **56**, 892 (1997).

[35] T. K. Ng and N. Nagaosa, Broken time-reversal symmetry in Josephson junction involving two-band superconductors, Europhys. Lett. **87**, 17003 (2009).

[36] Y. Asano, Y. Tanaka, M. Sigrist, and S. Kashiwaya, Josephson current in s-wave-superconductor/Sr_2RuO_4 junctions, Phys. Rev. B **67**, 184505 (2003).

[37] C. J. Trimble, M. T. Wei, N. F. Q. Yuan, S. S. Kalantre, P. Liu, H.-J. Han, M.-G. Han, Y. Zhu, J. J. Cha, L. Fu, and J. R. Williams, Josephson detection of time-reversal symmetry broken superconductivity in SnTe nanowires, npj Quantum Mater. **6**, 61 (2021).

[38] O. Can, T. Tummuru, R. P. Day, I. Elfimov, A. Damascelli, and M. Franz, High-temperature topological superconductivity in twisted double-layer copper oxides, Nat. Phys. **17**, 519 (2021).

[39] T. Tummuru, S. Plugge, and M. Franz, Josephson effects in twisted cuprate bilayers, Phys. Rev. B **105**, 064501 (2022).

[40] H.-P. Sun, S.-B. Zhang, C.-A. Li, and B. Trauzettel, Tunable second harmonic in altermagnetic Josephson junctions, Phys. Rev. B **111**, 165406 (2025).

[41] S. Shapiro, Josephson currents in superconducting tunneling: The effect of microwaves and other observations, Phys. Rev. Lett. **11**, 80 (1963).

[42] A. Barone and G. Paterno, *Physics and Applications of the Josephson Effect* (Wiley, New York, 1982).

[43] J. C. Cuevas, J. Heurich, A. Martín-Rodero, A. Levy Yeyati, and G. Schön, Subharmonic Shapiro steps and assisted tunneling in superconducting point contacts, Phys. Rev. Lett. **88**, 157001 (2002).

[44] M. Chauvin, The Josephson Effect in Atomic Contacts, Université Pierre et Marie Curie - Paris VI, 2005, https://theses.hal.science/tel-00107465v2.

[45] P. Kot, R. Drost, M. Uhl, J. Ankerhold, J. C. Cuevas, and C. R. Ast, Microwave-assisted tunneling and interference effects in superconducting junctions under fast driving signals, Phys. Rev. B. **101**, 134507 (2020).

[46] J. Siebrecht, H. Huang, P. Kot, R. Drost, C. Padurariu, B. Kubala, J. Ankerhold, J. C. Cuevas, and C. R. Ast, Microwave excitation of atomic scale superconducting bound states, Nat. Commun. **14**, 6794 (2023).

[47] We have fewer sites in the right lead as $\delta\Delta_R(t) \approx 0$. Additionally, it has a larger equilibrium gap $\Delta_{0,R} > \Delta_{0,L}$, and hence,

a shorter coherence length compared to the left lead ($\xi_{SC,R} < \xi_{SC,L}$).

[48] P. W. Anderson, N. R. Werthamer, and J. M. Luttinger, An additional equation in the phenomenology of superconductivity: Resistive effects, Phys. Rev. **138**, A1157 (1965).

[49] When the reference level for energies is set to the Fermi energy, the energy of the ground state with N and $N+2$ particles, differing by a pair, is the same. Relative to this reference level, in the presence of a potential V, the ground state with $N+2$ particles is lower in energy by 2 eV. Since $\Delta \sim \langle N|c_{-\mathbf{k}\downarrow}c_{\mathbf{k}\uparrow}|N+2\rangle$, it gathers an extra oscillation factor e^{i2eVt}. This argument follows Ref. [50].

[50] L. P. Gorkov, On the energy spectrum of superconductors, Sov. Phys. JETP **7**, 505 (1958).

[51] F. S. Bergeret, P. Virtanen, T. T. Heikkilä, and J. C. Cuevas, Theory of microwave-assisted supercurrent in quantum point contacts, Phys. Rev. Lett. **105**, 117001 (2010).

[52] V. Ambegaokar and A. Baratoff, Tunneling between superconductors, Phys. Rev. Lett. **10**, 486 (1963).

[53] A. I. Larkin and Y. N. Ovchinnikov, Tunnel effect between superconductors in an alternating field, Zh Eksp. Teor. Fiz. **51**, 1535 (1966) [Sov. Phys. JETP **25**, 1036 (1966)].

[54] V. Ambegaokar, U. Eckern, and G. Schön, Quantum dynamics of tunneling between superconductors, Phys. Rev. Lett. **48**, 1745 (1982).

[55] N. R. Werthamer, Nonlinear self-coupling of Josephson radiation in superconducting tunnel junctions, Phys. Rev. **147**, 255 (1966).

[56] A. Lahiri, S.-J. Choi, and B. Trauzettel, Nonequilibrium fractional Josephson effect, Phys. Rev. Lett. **131**, 126301 (2023).

[57] H. P. Ojeda Collado, G. Usaj, J. Lorenzana, and C. A. Balseiro, Fate of dynamical phases of a BCS superconductor beyond the dissipationless regime, Phys. Rev. B **99**, 174509 (2019).

[58] A. Kamenev, *Field Theory of Non-equilibrium Systems* (Cambridge University Press, Cambridge, England, 2011).

[59] M. P. Kemoklidze and L. P. Pitaevskii, Dynamics of a superfluid Fermi gas at finite temperatures, Zh Eksp. Teor. Fiz **50**, 243 (1966) [Sov. Phys. JETP **25**, 1036 (1966)].

[60] A. F. Volkov and S. M. Kogan, Collisionless relaxation of the energy gap in superconductors, Zh Eksp. Teor. Fiz **65**, 2038 (1974) [Sov. Phys. JETP, **38**, 1018 (1974)].

[61] V. L. Vadimov, I. M. Khaymovich, and A. S. Mel' nikov, Higgs modes in proximized superconducting systems, Phys. Rev. B **100**, 104515 (2019).

[62] M. Dzero, Collisionless dynamics of the pairing amplitude in disordered superconductors, Phys. Rev. B **109**, L100503 (2024).

[63] A. A. Abrikosov, L. P. Gorkov, and I. E. Dzyaloshinski, *Methods of Quantum Field Theory in Statistical Physics* (Dover, New York, 1975).

[64] P. G. de Gennes, *Superconductivity of Metals and Alloys* (Benjamin, New York, (1966).

[65] G. Stefanucci, E. Perfetto, and M. Cini, Time-dependent quantum transport with superconducting leads, J. Phys.: Conf. Ser. **220**, 012012 (2010).

[66] A. Levy Yeyati, A. Martín-Rodero, and F. J. García- Vidal, Self-consistent theory of superconducting mesoscopic weak links, Phys. Rev. B **51**, 3743 (1995).

[67] M. P. Samanta and S. Datta, Electrical transport in junctions between unconventional superconductors: Application of the Green's-function formalism, Phys. Rev. B **57**, 10972 (1998).

[68] J. C. Cuevas, A. Martín-Rodero, and A. Levy Yeyati, Hamiltonian approach to the transport properties of superconducting quantum point contacts, Phys. Rev. B **54**, 7366 (1996).

[69] A.-P. Jauho, N. S. Wingreen, and Y. Meir, Time-dependent transport in interacting and noninteracting resonant-tunneling systems, Phys. Rev. B **50**, 5528 (1994).

[70] T. Xu, T. Morimoto, A. Lanzara, and J. E. Moore, Efficient prediction of time- and angle-resolved photoemission spectroscopy measurements on a nonequilibrium BCS superconductor, Phys. Rev. B **99**, 035117 (2019).

[71] L. V. Keldysh, Diagram technique for nonequilibrium processes, Sov. Phys. JETP **20**, 1018 (1964).

[72] G. Stefanucci and R. van Leeuwen, *Nonequilibrium Many-body Theory of Quantum Systems: A Modern Introduction* (Cambridge University Press, Cambridge, England, 2013).

[73] S. A. González, L. Melischek, O. Peters, K. Flensberg, K. J. Franke, and F. von Oppen, Photon-assisted resonant Andreev reflections: Yu-Shiba-Rusinov and Majorana states, Phys. Rev. B **102**, 045413 (2020).

[74] M. Wimmer, Quantum Transport in Nanostructures: From Computational Concepts to Spintronics in Graphene and Magnetic Tunnel Junctions, Ph.D. thesis, Universität Regensburg, 2008.

[75] $G^< = (1+\Sigma^r G^r)g^<(1+G^a\Sigma^a) + G^r\Sigma^< G^a$. The first term refers to the initial conditions. In the presence of a finite lifetime $\sim 1/\Gamma$, it decays to zero before the bias voltage is applied due to the exponentially decaying $G^{r/a}$ [71–74].

[76] We do not find any significant $\cos(\phi(t))$ and $\cos(2\phi(t))$ currents.

[77] C. A. Hamilton and S. Shapiro, Experimental demonstration of the Riedel peak, Phys. Rev. Lett. **26**, 426 (1971).

[78] C. A. Hamilton, Frequency dependence of the Josephson current, Phys. Rev. B **5**, 912 (1972).

[79] K. K. Likharev, *Dynamics of Josephson Junctions and Circuits* (Gordon and Breach, New York, 1986).

[80] G. Marchegiani, L. Amico, and G. Catelani, Quasiparticles in superconducting qubits with asymmetric junctions, PRX Quantum **3**, 040338 (2022).

[81] T. Connolly, P. D. Kurilovich, S. Diamond, H. Nho, Charlotte G. L. Bøttcher, L. I. Glazman, V. Fatemi, and M. H. Devoret, Coexistence of nonequilibrium density and equilibrium energy distribution of quasiparticles in a superconducting qubit, Phys. Rev. Lett. **132**, 217001 (2024).

[82] M. McEwen, K. C. Miao, J. Atalaya, A. Bilmes, A. Crook, J. Bovaird, J. M. Kreikebaum, N. Zobrist, E. Jeffrey, B. Ying, A. Bengtsson, H.-S. Chang, A. Dunsworth, J. Kelly, Y. Zhang, E. Forati, R. Acharya, J. Iveland, W. Liu, S. Kim, *et al.*, Resisting high-energy impact events through gap engineering in superconducting qubit arrays, Phys. Rev. Lett. **133**, 240601 (2024).

[83] H. Nho, T. Connolly, P. D. Kurilovich, S. Diamond, C. G. L. Bøttcher, L. I. Glazman, and M. H. Devoret, Recovery dynamics of a gap-engineered transmon after a quasiparticle burst, Phys. Rev. Lett. (2026).

[84] W. M. van Weerdenburg, A. Kamlapure, E. H. Fyhn, X. Huang, N. P. van Mullekom, M. Steinbrecher, P. Krogstrup, J. Linder, and A. A. Khajetoorians, Extreme enhancement of superconductivity in epitaxial aluminum near the monolayer limit, Sci. Adv. **9**, eadf5500 (2023).

[85] O. A. E. Cherney and J. Shewchun, Enhancement of superconductivity in thin aluminium films, Can. J. Phys. **47**, 1101 (1969).

[86] N. A. Court, A. J. Ferguson, and R. G. Clark, Energy gap measurement of nanostructured aluminium thin films for single Cooper-pair devices, Supercond. Sci. Technol. **21**, 015013 (2008).

[87] A. Altland and B. D. Simons, *Condensed Matter Field Theory* (Cambridge University Press, Cambridge, England, 2010).

[88] E. Ben-Jacob, E. Mottola, and G. Schön, Quantum shot noise in tunnel junctions, Phys. Rev. Lett. **51**, 2064 (1983).